

Fall 2013

A Statistical Analysis for Estimating Fish Number Density with the Use of a Multibeam Echosounder

Madeline L. Schroth-Miller
University of New Hampshire, Durham

Follow this and additional works at: <https://scholars.unh.edu/thesis>

Recommended Citation

Schroth-Miller, Madeline L., "A Statistical Analysis for Estimating Fish Number Density with the Use of a Multibeam Echosounder" (2013). *Master's Theses and Capstones*. 801.
<https://scholars.unh.edu/thesis/801>

This Thesis is brought to you for free and open access by the Student Scholarship at University of New Hampshire Scholars' Repository. It has been accepted for inclusion in Master's Theses and Capstones by an authorized administrator of University of New Hampshire Scholars' Repository. For more information, please contact nicole.hentz@unh.edu.

A Statistical Analysis for Estimating Fish Number
Density with the Use of a Multibeam Echosounder

BY

MADELINE L. SCHROTH-MILLER

B.S., California Polytechnic State University, 2009

THESIS

Submitted to the University of New Hampshire
in partial fulfillment of
the requirements for the degree of

Master of Science

in

Mathematics: Applied Mathematics

September 2013

UMI Number: 1524298

All rights reserved

INFORMATION TO ALL USERS

The quality of this reproduction is dependent upon the quality of the copy submitted.

In the unlikely event that the author did not send a complete manuscript and there are missing pages, these will be noted. Also, if material had to be removed, a note will indicate the deletion.



UMI 1524298

Published by ProQuest LLC 2013. Copyright in the Dissertation held by the Author.

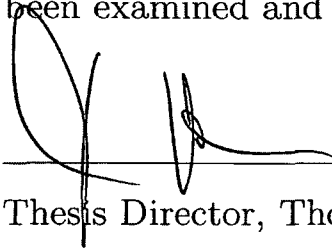
Microform Edition © ProQuest LLC.

All rights reserved. This work is protected against unauthorized copying under Title 17, United States Code.

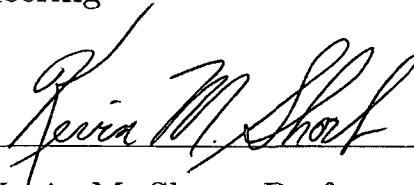


ProQuest LLC
789 East Eisenhower Parkway
P.O. Box 1346
Ann Arbor, MI 48106-1346

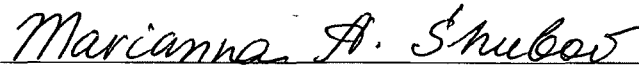
This dissertation has been examined and approved.



Thesis Director, Thomas C. Weber
Research Assistant Professor of Ocean Engi-
neering



Kevin M. Short, Professor of
Mathematics



Marianna A. Shubov, Professor of
Mathematics

Date

DEDICATION

To my love, thank you for being my rock.

ACKNOWLEDGMENTS

Thank you to Hunter Glanz, Kevin Jerram, and Matt Morena for your continued guidance and support. I greatly appreciate all of the help you provided me. To my committee, I would like to thank you for all of the help and patience you have shown me.

TABLE OF CONTENTS

	Page
DEDICATION	iii
ACKNOWLEDGMENTS	iv
LIST OF FIGURES	vii
ABSTRACT	ix
CHAPTER	
1. INTRODUCTION	1
1.1 Traditional Methods for Estimating Fish Number Density	4
1.2 DSH Model	6
1.3 Goal of Paper	10
2. EXPLORATION OF DSH MODEL ASSUMPTIONS	12
3. DSH MODEL WITH NOISE	19
3.1 Noise Model Variations	22
4. EXAMPLE WITH JUVENILE ATLANTIC BLUEFIN TUNA	29
4.1 Experiment Description	30
4.2 Estimate Fish Number Density	32
5. DISCUSSION	41

6. FIGURES	46
BIBLIOGRAPHY	59
APPENDICES	
A. DERIVATION OF AVERAGE NUMBER OF FISH (PER RESOLUTION CELL)	63
B. DERIVATION OF PROBABILITY DENSITY FUNCTION OF THE FISH SCATTERING STATISTIC AND BEAM PATTERN MODULATION	71
C. VARIANCE OF $\langle N \rangle$	77

LIST OF FIGURES

Figure	Page
6-1 Environmental setup for the simulations conducted and data analyzed. The number of contributors for a given resolution cell are determined by the hemi-ellipsoidal shell encompassing the school at some range r with a thickness determined from the pulse length, τ , and sound speed, c . On average, the shell can be approximated by an 11° by 11° hemi-ellipsoidal shell.	46
6-2 Geometry of the backscattering measurements. The change in volume is represented by $dV = R^2 \sin(\phi) dR d\phi dv$ where ϕ is the elevation angle and v is the rotational angle.	47
6-3 (a) Change in fourth normalized moment of $b(v, \phi)$ for varying elevation angles (ϕ). (b) Ratio of the fourth normalized moment of $b(v, \phi)$ to volume for varying elevation angles. The blue curves represent the Mills Cross 1° by 0.5° transducer and the red curves represent the 7° transducer. For small elevation angles in (a), numerical error arises.	48
6-4 Estimates of the average number of fish per resolution cell, $\langle N \rangle$. A Mills Cross 1° by 0.5° transducer is simulated with an elevation angle, ϕ , equal to 5.5° . The true estimate of $\langle N \rangle$ is equal to 25 fish per resolution cell.	49
6-5 Error estimates in $\langle N \rangle$. (a) Variance of $\langle N \rangle$. (b) Absolute percent change in $\langle N \rangle$ from the true value.	50
6-6 Experimental setup for the data collected. (a) Aerial image of the ABFT school with the side-looking 400 kHz MBES. (b) A single ping from the multibeam showing a vertical cross-section of the school.	51

- 6-7 Probability Density Function of $b(v, \phi)$ from a Mills Cross 1° by 0.5° transducer. The rotational angle, v , ranges from 0 to 360° . The elevation angle, ϕ , is restricted between 0 and 5.5° . A centered beam (red line), a 1.83° steered beam (yellow line), a 2.75° steered beam (green line), a 3.67° steered beam (magenta line), and a 5.5° steered beam (blue line) are simulated. The fourth normalized moments of each beam are represented. 52
- 6-8 Scintillating index of intensity (SI) over 124 pings. (a) Raw estimates of SI. (b) Smoothed estimates of SI with a box car filter over 100 samples and 2 beams. SI is a unitless parameter. The red box represents the boundary of the fish school. 53
- 6-9 Smoothed scintillating index of intensity represented in cartesian coordinates (over 124 pings). The hypothesized surface is represented by the horizontal black line. 54
- 6-10 Unsmoothed scintillating index of the noise contribution, $\frac{\langle (MM^*)^2 \rangle}{\langle MM^* \rangle^2}$, found over 124 pings of target-absent data. 55
- 6-11 (a) $\langle N \rangle$ estimate from the DSH model (Eq. 1.3). (b) $\langle N \rangle$ estimate from the variant model (Eq. 3.5). Both are found over a smoothed SI. The red box represents the boundary of the fish school. Units of $\langle N \rangle$ are in fish per resolution cell. 56
- 6-12 Ratio of the variance of the variant model (Eq. 3.5) to the variance of the DSH model (Eq. 1.3), i.e. $Var(\langle N \rangle_{Eq.3.5})/Var(\langle N \rangle_{Eq.1.3})$ 57
- 6-13 Multiple sound paths between the sonar and fish. (a) Direct path. (b) Reflection from the surface to the fish and back to the sonar. (c) Reflection from the fish to the surface and back to the sonar. (d) Reflection to the surface, then the fish, back to surface, with a return to the sonar. 58
- B-1 1. Geometry of backscattered pressure signal for setup number one. 2. Vertical slice of cylindrical shape used to find area. 76
- B-2 Geometry of backscattered pressure signal for setup number three. 76

ABSTRACT

A Statistical Analysis for Estimating Fish Number Density with the Use of a Multibeam Echosounder

by

MADLINE L. SCHROTH-MILLER

University of New Hampshire, September, 2013

Fish number density can be estimated from the normalized second moment of acoustic backscatter intensity [Denbigh et al., J. Acoust. Soc. Am. 90, 457-469 (1991)]. This method assumes that the distribution of fish scattering amplitudes is known and that the fish are randomly distributed following a Poisson volume distribution within regions of constant density. It is most useful at low fish densities, relative to the resolution of the acoustic device being used, since the estimators quickly become noisy as the number of fish per resolution cell increases. New models that include noise contributions are considered. The methods were applied to an acoustic assessment of juvenile Atlantic Bluefin Tuna, *Thunnus thynnus*. The data were collected using a 400 kHz multibeam echo sounder during the summer months of 2009 in Cape Cod, MA. Due to the high resolution of the multibeam system used, the large size (approx. 1.5 m) of the tuna, and the spacing of the fish in the school, we expect there to be low fish densities relative to the resolution of the multibeam system. Results of the fish number density based on the normalized second moment of acoustic intensity are compared to fish packing density estimated using aerial imagery that was collected simultaneously.

CHAPTER 1

INTRODUCTION

Understanding the impacts or effects of natural and anthropogenic influences on fish populations is critical to the ecosystem the fish is a part of, the well-being of the species itself and the fishery dependent upon it. Intended and incidental impacts such as habitat destruction and mortality of non-target species have resulted in overexploitation of fish populations and degradation of pivotal ecosystems that provide for the fish communities (Pikitch *et. al.* 2004) [30]. Maintaining the stability of an exploited resource is crucial and can be achieved with specific information about the stock. Modern fisheries stock assessments provide extensive information and technical advice to maintain the productivity of fish stocks and allow for more effective fisheries and enhanced management of endangered species (Cadima 2003) [4]. Understanding the trend of how school sizes change over time is a simple way of estimating the effects on a fish population. This can be done multiple ways through a fish stock assessment. Stock assessment methods incorporate a variety of tools that are both fishery dependent and independent. Data collected from recorded landings (amount of fish caught and sold per year), portside sampling, and vessel-monitoring

surveys are reliant on the fishery; whereas trawls, seines, video and acoustic surveys can all be conducted without any fishing activity (Cooper 2006) [9]. Since it is more difficult for scientists than for fisherman to collect large amounts of samples in expansive areas continuously over time, fishery-independent surveys are greatly depended upon (Wallace and Fletcher 2001) [42]. Also, fishery-dependent surveys may possibly have insufficient and biased catch information which is undesirable by the scientific community (Patterson *et. al.* 2001) [27]. In particular, the use of acoustic surveys in fisheries has become widespread to circumvent the limitations of traditional survey methods and to provide additional information about fish density, spatial distribution, and behavior of fish schools (Gurshin *et. al.* 2009) [20]. Acoustic instruments that transmit and receive sound waves are more capable of detecting fish than any visual system since the penetration of sound in water is exceptionally greater than light (Fernandes *et. al.* 2002) [15]. Of the techniques used in fisheries acoustics, multi-beam echo sounders (MBES) are a relatively new tool being implemented. Due to the potentially high cost and lack of dynamic range associated with multibeams, they are not traditionally used in fisheries science but have great potential. Traditional echo sounders used in acoustic fish surveys are limited in the estimation of geometrical parameters of the fish school due to the possible effects of vessel avoidance (Soria *et. al.* 2003 and Cutter and Demer 2007) [34, 10], inaccurate volume estimations (Gerlotto *et. al.* 1999) [19], and restrictions to a two-dimensional plane (Mayer *et. al.* 1999)

[25]. Studies have been conducted to determine the usefulness of implementing a 3D sonar system (including a MBES) in estimating the shape and biomass of fish schools without experiencing the disadvantages of traditional sonars and have had promising results (Weber *et. al.* 2009 and Gurshin *et. al.* 2009) [44, 20]. Fish school surveys using multibeam sonars have been conducted in shallow waters with the use of video image analysis to estimate school structure and behavior (Gerlotto *et. al.* 2000) [17], estimates of the distribution of densities within a school have been explored (Gerlotto and Paramo 2003) [18], and a description of the capabilities of a MBES in estimating target strength and volume backscattering strength through analytical and empirical methods has been done (Cochrane *et. al.* 2003) [8]. New methods of data acquisition have been explored (Brehmer *et. al.* 2006) [3] and the effects of a new MBES specifically intended for fisheries assessment has been examined (Trenkel *et. al.* 2008) [39]. Most of these studies have shown improvements on the estimates being found when using a multibeam echosounder, however the use of such tools does not provide precise measurements and biases still exist due to potential noise complications, calibration issues, irregular school shapes, and a potential lack of knowledge about fish location and orientation within a beam.

1.1 Traditional Methods for Estimating Fish Number Density

Two commonly used methods for estimating the number density of fish aggregations with acoustic sonar systems are echo-counting and echo-integration (Simmonds and McLennan 2005) [33]. If the individual echoes on an echogram can be distinguished from one another and the assumptions that each echo is produced by one fish and the fish are randomly distributed are satisfied, then the number of fish in a given area can be determined by counting the total number of echoes present, i.e. echo-counting. If the density of fish is too high to detect individual echoes then echo-integration is a comparable alternative that is frequently used. An estimate for the density of fish from echo-intensity is determined by summing or integrating the energy, or equivalently the echo intensity, over certain parts of the echogram. The energy for a given time period is equal to the integral of the magnitude of the voltage, produced by the echosounder, squared. The fish number density (fnd) is then found from the average of the echo-integrals from a collection of transmitted pings (Simmonds and McLennan 2005) [33].

As addressed by Simmonds and McLennan [2005] [33], there are certain drawbacks and limitations in using the traditional methods for estimating fish abundance. Calibration of the transducer and the instruments used to convert pressure amplitude measurements to electrical signals is needed. In order to obtain more accurate estimates of fish number density, the method of calibration proposed by Foote *et. al.*

[1987] [16] should be implemented. Also, an estimate of the target strength of a fish in their natural environment, defined as the ratio of scattered intensity at a reference of 1 m to the incident intensity (Pierce 1981) [29], may have a variable amount of uncertainty associated with it due to the possible presence of multiple species, the sporadic changes in orientation of the fish in the beam (Urick 1983) [40], and the conceivably large range of fish sizes resulting in a wide spread of the target strength distribution. Various methods for estimating fish number density have been examined in order to circumvent the drawbacks of conventional methods.

Statistics of acoustic backscatter have been explored in depth and used to estimate density of scatterers in a number of fashions. The statistical analysis of non-Rayleigh echo amplitudes from seafloor backscatter has been examined (Stanic and Kennedy 1993 and Lyons and Abraham 1999) [36, 24] with extensive research conducted in determining possible distributions to describe the echo statistics of reverberation (Abraham and Lyons 2002) [1]. Such methods have been utilized to describe the echo statistics of patch scatterers and individual scatterers from both fish and seafloor contributors (Stanton and Clay 1986, Chu and Stanton 2010, and Stanton and Chu 2010) [38, 5, 37]. Estimating density of acoustic point scatterers in volume reverberation has been done using recursive algorithms (Ehrenberg 1972) [13], empirical estimations (Jobst and Smits 1974) [14], and by examining level crossing data (Spindel and McElroy 1973) [35]. The concepts of fluctuations in single-interval statistics

have the potential for application in medical tissue characterization (Waag *et. al.* 1982) [41] and have been used to estimate density of scatterers, such as light scatterers (Pusey *et. al.* 1974) [31], within mediums similar to and including course-grained glass (Bluemel *et. al.* 1972) [2]. Fish estimation models involving fluctuations of the returned signal defined by high order (power of 2 or more) statistical moments of backscattered intensity have been examined (Wilhelmij and Denbigh 1984 and Denbigh *et. al.* 1991) [45, 11] and will be used frequently in this paper. The established model for the estimate of fish number density that is the basis of this research will be referred to as the DSH model which is explored in depth in Denbigh *et. al.* [1991] [11].

1.2 DSH Model

When the number of independent contributors in the returned acoustic pressure signal is small there is a deviation from Gaussian statistics. Estimates of fish number density can be made under the assumption of non-Gaussian statistics. The estimate of n_{fd} is defined as the number of fish per meter cubed, ρ . This is found by taking the estimate for the average number of fish per resolution cell, $\langle N \rangle$, and dividing out by the volume considered in the estimation. The scatterers contributing to a resolution cell are within the hemi-spherical shell determined by some range value, the speed of sound in the medium, and the pulse length of the system being used. The volume that encompasses the scatterers is determined by the boundaries of the

school at some range and will be used to estimate the fish number density. This setup can be seen in Figure 1. Knowledge of the second normalized moment of intensity, $\frac{\langle I^2 \rangle}{\langle I \rangle^2}$, i.e. the scintillating index (SI), is needed in order to determine the average number of fish for a resolution cell of an ensonified volume. The SI represents the fluctuation of intensity of the scatterer in time and/or space. Within the DSH model for estimating fish number density, the SI describes the fluctuations of fish scatterer intensities by way of variations in fish location and attitude in the sonar beam. The acoustic echo, P , contains the random amplitude and phase, A and θ respectively, scattered from a total of N fish:

$$P = \sum_{j=1}^N A_j e^{i\theta_j}. \quad (1.1)$$

The model in Wilhelmij and Denbigh [1984] [45] was redefined as the DSH model by introducing multiple factors in the amplitude, A . In Eq. (1.1) A_j is a function of three components: (a) the effects of fish scattering, a_j , (b) beam pattern fluctuations, b_j , and (c) pulse envelope changes, c_j ; such that $A_j = a_j b_j c_j$. The beam pattern itself does not fluctuate but it is determined by the random locations of the fish within the beam and the area of ensonification. Since the location of the scatterer with respect to the main response axis of the beam is random, the angles that determine the beam pattern value (i.e. rotational angle, ν , and elevation angle, ϕ) at the fish's location are therefore random, thus defining the beam pattern contribution from the j^{th} fish

to be a random variable. The angle definitions can be seen in Figure 2. For simplicity purposes, the effects of the random locations of fish on the beam pattern values will be referred to as the beam pattern fluctuations. Intensity for each resolution cell is found by obtaining the square of the magnitude of the pressure (Eq. 1.2):

$$I = PP^* = |P|^2. \quad (1.2)$$

In estimating how many contributors there are in the signal, the first and second moments of intensity are found and manipulated to produce the average number of fish per resolution cell, $\langle N \rangle$ (Denbigh *et. al.* 1991) (See Appendix A):

$$\langle N \rangle = \frac{\langle A^4 \rangle}{\langle A^2 \rangle^2} \left[\frac{\langle I^2 \rangle}{\langle I \rangle^2} - 2 \right]^{-1}. \quad (1.3)$$

The components of the amplitude are random variables with assumed or empirically derived distributions. The probability density functions (pdf) of the components of the signal amplitude and phase for a fish scatterer are discussed in depth later and explicitly derived in Appendix B.

The success of this model is contingent on divergence from Gaussian statistics in the return signal. On the basis of the Central Limit Theorem, Gaussian statistics occur when the scattered signal contains the sum of many independent contributions (Pusey *et. al.* 1974) [31]. Information about the average fish number density cannot

be extracted from the statistics in the Gaussian limit. If the pressure signal returned is complex Gaussian,

$$P = X + iY \text{ where } X, Y \sim N(\mu, \sigma) \quad (1.4)$$

then the resulting intensity,

$$I = PP^* = X^2 + Y^2, \quad (1.5)$$

will be Chi-squared distributed with two degrees of freedom. In such a case, the second normalized moment of intensity will equal two and therefore cause the model to diverge. In order to obtain estimates for the average number of fish that have small associated variances, the scintillating index of the intensity must differ from two which requires the number of fish per resolution cell to be low. Since higher order moments are being considered in the estimation of $\langle N \rangle$ a large amount of samples in space and/or time must be used in order to get a better description of the pdf. If only a few samples have been taken to estimate the moments of a heavily peaked distribution there may be a resulting bias in the estimate of the moments since the peak may or may not be accurately represented in the calculation. Another possible source of error in the DSH model may come from the assumption that all noise is negligible. However, the information needed to implement this statistical method (DSH model) may be more attainable than the information that is needed

for other techniques, such as scattering information and target strength of a particular species. Along with this, the drawbacks of the DSH method (i.e. the possible incorrect noise assumption, the required low number count and the need for a large amount of samples) can be addressed by using a different transducer to image the fish school and by making different assumptions. The requirement to know the target strength for traditional methods is unnecessary for the DSH model and the system used to ensonify the school does not need to be calibrated due to the normalization of the moments. Additionally, the difficulty in satisfying the requirement of a low number of fish can be mitigated with a multibeam echosounder, or a narrow beam system in general. Since the area of maximum sensitivity is small for a narrow beam system, the number of contributions to the signal will inherently be small. In general, if the system's pulse length is small compared to the fish length, an expected low number of fish will be seen within an individual pulse since the many individual scattering points along the fish will come together and be considered as one scatterer. Using a MBES along with a small pulse length can achieve good range resolution as well. Thus a MBES would be a suitable complement to the DSH model.

1.3 Goal of Paper

In this paper the assumptions made for the random variables of the DSH model will be addressed and modified for the purposes of this research. The hypotheses further developed in this paper regarding the fish scattering amplitude distribution,

beam pattern fluctuation, and pulse envelope effects on the estimate of the average number of fish per resolution cell will be discussed. The DSH model assumed that the contribution from noise components in the signal was negligible. Possible sources of noise may include scatterers other than the targets of interest in the ensonified volume, electrical interference, mechanical boat noise, bubble build up on the transducer face, wind and surface effects and volume reverberation. The contributions to the signal from such sources could be important factors to consider depending on the circumstances of the experiment. Due to the range of possible noise source contributions, a modified DSH model that includes random white noise will be presented. In order to preserve the benefits of the DSH method (such as an uncalibrated system and minimal assumptions of the fish scattering characteristics) in conjunction with obtaining more accurate estimates of fish number density at high noise levels, variations of the complete noise model will be considered. Simulations of each model will be implemented in order to estimate the uncertainty associated with each model. The models will then be tested using Atlantic Bluefin Tuna data collected with a 400 kHz multibeam echosounder with a beam width of 1° by 0.5° . Estimates of the average number of fish per resolution cell and fish number density will be found and the uncertainty associated with such estimates and other sources of error will then be discussed.

CHAPTER 2

EXPLORATION OF DSH MODEL ASSUMPTIONS

Assumptions about the distributions of each of the random variables present in the received pressure signal are made in the DSH model in order to determine the average number of fish per resolution cell and the resulting fish number density. Since the number of fish takes on discrete non-negative integer values, the total number is assumed to follow a Poisson distribution. Along with this, since an individual fish contributor is assumed to be anywhere within the scattering volume and independent of the other scatterers, the phase, which is independent of the amplitude, is assumed to be uniform on the interval $[0, 2\pi]$ (Pusey *et. al.* 1974) [31]. In order for the spatial structure of the school to affect the distribution of the phase contributions, the fish would need to maintain spatial organization on the order of a wavelength or less. A change from the uniform assumption would require the implementation of much lower frequencies than those used here. Described in Clay and Medwin [1977] [6], if the number of scatterers along an individual fish body is large then the fish scattering amplitude distribution, A , is assumed to be Rayleigh, or in some cases Rician (Denbigh *et. al.* 1991) [11], since the convergence of the Central Limit Theorem creates

a complex Gaussian pressure signal (Wilhelmij and Denbigh 1984) [45]. The DSH model assumes the number of contributors to be low and thus inherently assumes a contributor is equivalent to one fish even though a sonar system with a wavelength smaller than the fish size would produce multiple scattering points along the body. According to Rice [1945] [32] and Clay and Heist [1984] [7], the Rician pdf is derived from the superposition of many random disturbances (narrow band passed noise) with sinusoidal components. Coherent backscatter from the swim bladder contributes to the sine wave, while the distributed component is due to scattering centers on the body and skeleton of the fish (Denbigh *et. al.* 1991) [11]. The underlying parameter, γ , of the Rician distribution is a ratio of the sine wave power to noise power (Eq. 2.1) where σ_c is the concentrated scattering component, σ_d is the distributed scattering component, and σ_{bs} , the sum of the two, is the backscattering cross section (Clay and Heist 1984) [7]:

$$\gamma = \frac{\sigma_c}{\sigma_d}, \text{ where } \sigma_{bs} = \sigma_c + \sigma_d. \quad (2.1)$$

This ratio describes the fish echoes and is dependent on the morphology and behavior of an individual within the area of ensonification. The ratio of the length of the fish to acoustic wavelength along with the fish movement can be directly related to the Rician parameter γ . According to Clay and Heist [1984] [7], if the length of the fish is relatively large to the wave length, i.e. $L/\lambda \geq 16$, the distributed

component will be the dominating factor resulting in a very small parameter γ . The experiments conducted in Clay and Heist [1984] [7] showed that as the movement of the fish increased, the parameter would decrease towards zero. A convergence to zero would reduce the Rician distribution to a Rayleigh distribution. Huygens wavelet theory (Clay and Medwin 1977) [6] help reinforce the Rayleigh assumption. At high frequencies, the phases of the wavelet sources depend on the attitude of the fish in the wavefield. If the fish is alive there will be many fluctuations in the signal. Compared to the whole fish, the swimbladder will not be a substantial contributor to the signal if the frequency is much higher than the resonance frequency (Love 1978) [22]. For the reasons stated above and prior knowledge about the relative size and schooling behavior of the fish present in the data collected, a Rayleigh distribution is assumed for the fish scattering statistic, a , thus resulting in a fourth normalized moment of two.

The characteristics of the pulse envelope do not influence the estimate of $\langle N \rangle$ for the research done here. A detailed description of the moments of the pulse envelope can be found in Denbigh *et. al.* [1991] [11]. However, since the fourth normalized moment of a short rectangular pulse envelope is equal to one, and a similar pulse was used in the work done here, the estimate of $\langle N \rangle$ for the data simulated and collected does not include the statistical moments of the pulse envelope.

As mentioned earlier, the beam pattern itself does not fluctuate, however, it is determined by the random locations of the fish within the beam and the area of ensonification. The importance of the beam pattern comes from understanding the differences between the returned signal from varying fish locations within the ensonified volume. A large fish located in the direction of a side lobe may produce the same signal strength as a small fish located in the main lobe. Thus, understanding the pdf of the beam pattern can provide insight into the backscattering strength and/or fish location within the volume. Depending on the sonar system used, an analytical form for the pdf of the beam pattern may not exist. The DSH model utilized an approximate formulation of the n^{th} moment derived in Lozow [1981] [23] to determine the standardized moments under the assumption that the distribution of fish within the ensonified volume is uniform. A method for empirically determining the pdf of the beam pattern with axial symmetry about the main axis is first presented in Peterson *et. al.* [1976] [28] and further discussed in Clay and Medwin [1977] [6]. An extended formulation of the distribution of a beam pattern with two angle dependencies can be found in Appendix B. To estimate the effects from a beam pattern that is similar to a MBES setup a Mills Cross, 1° by 0.5° , sonar system is simulated with a frequency equal to 400 kHz. A Mills Cross setup requires the two separate transducer arrays (i.e. transmit and receive array) to be perpendicular to one another. The sound emitted from each array will be narrow in one direction and wide in the other with the output

of the two producing a small directed area of sensitivity in post-processing. The beam pattern of a Mills Cross transducer will be the same as a rectangular array of similar dimensions (Urick 1983) [40]. Since the combined transmit and receive beam (1° by 0.5°) used in this paper is much narrower than the beam formed in Denbigh *et. al.* [1991] [11], the fourth normalized moments will randomly vary. The total area of ensonification and the assumption that scatterers are uniformly distributed heavily influence the outcome of the standardized moments of the beam pattern, $b(\nu, \phi)$. The assumption in the DSH model is that the fish scatterers are uniformly distributed over a hemispherical shell. For the narrow beam simulated in this paper, under the above assumptions, a fourth normalized moment is determined to be 15,472 differing by a factor of 65 from the DSH formulation of 237. This is consistent with the results expected from analyzing a very narrow beam. As the number of sidelobes increases the likelihood of seeing a small value in $b(\nu, \phi)$ increases resulting in high probabilities. Conversely, large values of $b(\nu, \phi)$ are less frequent and therefore associated with small probabilities. Under these circumstances high peaks and a heavy tail are formed in the creation of the $b(\nu, \phi)$ pdf of a Mills Cross 1° by 0.5° transducer. As found above, the fourth normalized moment emphasizes such peaks therefore resulting in very large values such as 15,472. This can be seen in Figure 3a.

Estimating fish number density with a Mills Cross 1° by 0.5° transducer can be difficult to do and error prone depending on the volume being ensonified. Since sound

spreads spherically, the volume covered by the MBES is the entire hemispherical shell determined by the distance from the scatterer, the pulse length of the sonar system, and the sound speed. However, the backscattered signal comprising of fish scattering may not have originated from every point within the hemispherical shell. In fact, for the studies conducted here, it is known that the fish are not present within the entire hemispherical shell. Determining the volume in which the fish are present is important to help ensure an estimate of $\langle N \rangle$ with a smaller variance. The fnd estimates are determined by dividing the estimate of $\langle N \rangle$ by the ensonified volume. Since the fourth normalized moment of the beam pattern is directly related to the volume by the elevation angle ϕ , the changes in volume coverage affect the estimate of fnd which is proportional to the ratio of the fourth normalized moment of the beam pattern to the volume. Figure 3b demonstrates such changes with varying coverage along with a comparison to a 7° Piston transducer. For both transducers, the ratio described is compared against varying volumes that are defined by the angle, ϕ , from the main response axis. The areas of concern are where the curves display steep slopes. For both transducers, changes in angle where the elevation angle is less than 10° will produce increasingly different ratios. For example, a 1° difference from an elevation angle of 60° would produce a 0.45% change in the ratio described, whereas a 1° difference from an elevation angle of 4° would produce a 1.8% change in the value of the ratio. Also, as seen in Figure 3a, the difference in the fourth normalized

moment of the beam pattern of the Mills Cross transducer is much greater at small elevation angles resulting in the sharp changes and steep slopes in the ratio described (Figure 3b). The differences in fnd described by the ratio of the fourth normalized moment of the beam pattern to the volume are much more impacting with changes in volume defined by small elevation angles than with volumes determined by large elevation angles. Thus, understanding the spatial distribution of the fish and the total volume ensonified is important in estimating the effects of beam pattern fluctuations on the average number of fish per resolution cell and therefore fish number density. Finally, the DSH model assumes that all possible sources of noise are negligible in the estimation of average number of fish.

CHAPTER 3

DSH MODEL WITH NOISE

The DSH model assumes that interference from noise contributions such as volume and sea-surface reverberations, and electrical interference are negligible. In order to address the potential presence of noise for a given situation, we derive a new model that includes a complex Gaussian white noise component. This new model will be referred to as the DSH-N model. The noise contribution can stem from multiple sources and can be environmentally produced and/or manufactured within the sonar system used. It is assumed that the noise follows a complex Gaussian distribution since it is believed that it is constructed from a large number of random processes. The new backscattered pressure signal including noise takes the following form,

$$P_M = \sum_{j=1}^N A_j e^{i\theta_j} + M, \quad (3.1)$$

where N is the number of contributors (assumed to be the total number of fish), A_j and θ_j are the signal amplitude and phase of the j^{th} contributor, and M is a single noise component uncorrelated to the scattered pressure signal from the fish. The first

and second moments of intensity are then found to help determine an estimate for the average number of fish, $\langle N \rangle$. The derivation of the first moment of intensity,

$$\langle I \rangle = \langle PP^* \rangle = \langle N \rangle \langle A^2 \rangle + \langle MM^* \rangle, \quad (3.2)$$

and the second moment of intensity,

$$\begin{aligned} \langle I^2 \rangle = \langle (PP^*)^2 \rangle = & \langle N \rangle \langle A^4 \rangle + 2 \langle N \rangle \langle A^2 \rangle \langle N \rangle \langle A^2 \rangle \\ & + 2 \langle N \rangle \langle A^2 \rangle \langle MM^* \rangle + \langle (MM^*)^2 \rangle, \end{aligned} \quad (3.3)$$

can be found in Appendix A. A new normalized parameter including the first and second moments of backscattered intensity and noise are manipulated to find the the average number of fish per resolution cell for the DSH-N model:

$$\langle N \rangle = \left[\frac{\langle A^4 \rangle}{\langle A^2 \rangle^2} + 4 \frac{\langle MM^* \rangle}{\langle A^2 \rangle} \right] \left[\frac{\langle I^2 \rangle - \langle (MM^*)^2 \rangle}{(\langle I \rangle - \langle MM^* \rangle)^2} - 2 \right]^{-1}. \quad (3.4)$$

Although the new noise model accounts for multiple, possibly unknown, sources of noise that are unaccounted for in the DSH model, there are some disadvantages in using the DSH-N model, Eq. (3.4). As mentioned earlier, an appealing aspect of the DSH model is that it doesn't require information of the fish target strength and that an uncalibrated sounder can be used. If in Eq. (3.4) the noise is considered to be non-negligible, these advantages of the DSH model would disappear. Embedded within

the received amplitude of the signal are the aforementioned random variables of fish scattering amplitude, transmitted and received beam pattern fluctuations and pulse shape fluctuations. However, transmitted and received calibration coefficients needed to correct for errors when transforming voltage measurements to pressure measurements are also present in the signal. Due to the nature of the signal and depending on the type of noise embedded within the signal, these coefficients may cancel out in the normalization of the intensity. If the noise is due to volume reverberation, then the calibration coefficients in the pressure signal amplitude of the scatterers are also present in the noise component and are therefore canceled out in the normalization. However, if the noise comes from a different source (i.e. electronic self-noise), then it is important to either use a calibrated system, or be able to quantify the uncertainty in the estimates due to the coefficients' presence (since the noise is considered strictly electrical noise). For the purposes of this research, the noise is considered to be volume reverberation and the calibration coefficients can therefore be disregarded. This new noise model also requires more knowledge about the fish scattering statistics. In the numerator of Eq. (3.4), due to the presence of the second moment of the signal amplitude, $\langle A^2 \rangle$, in the latter portion of the numerator, an estimate of the parameters of the distribution for the fish scattering statistic would need to be made. Obtaining this estimate may be just as difficult as acquiring the target strength of

the fish and would most likely negate the benefits gained from using the DSH model to estimate fish number density.

3.1 Noise Model Variations

In order to incorporate some aspect of noise within the DSH model without negating its benefits, variations of the model are developed and simulated. The simulations are conducted to estimate the average number of fish per resolution cell for varying values of noise contributions. The true average is specified to be 25 fish. The school is set 45 meters away from the sonar encompassing an 11° by 11° hemi-ellipsoidal shell with thickness determined by the pulse length and speed of sound, $c\tau/2$. As mentioned earlier, this setup can be seen in Figure 1. The Mills Cross 1° by 0.5° beam is centered towards the middle of the school and calculations of the pdf of the beam pattern are empirically found by restricting the elevation angle ϕ to 5.5° , which is determined by the dimensions of the school. Since the fourth normalized moment of the Rayleigh distribution is equal to 2 regardless of the parameter used, the contribution of the fish scattering statistic is set to be 2. The estimate for the SI and resulting average number of fish per resolution cell, $\langle N \rangle$, is derived from 20 ensembles containing 10,000 simulated samples/pings each. The DSH model (Eq. 1.3), the DSH-N model (Eq. 3.4) and two “variants” of the noise model (Eq. 3.5 and Eq. 3.6) are compared using signal to noise ratio (SNR) in order to determine the

most suitable method to implement with the tools utilized. SNR is defined as the ratio of intensities measured in decibels. The model defined by Eq. 3.5,

$$\langle N \rangle = \frac{\langle A^4 \rangle}{\langle A^2 \rangle^2} \left[\frac{\langle I^2 \rangle - \langle (MM^*)^2 \rangle}{(\langle I \rangle - \langle MM^* \rangle)^2} - 2 \right]^{-1} \quad (3.5)$$

is the first variant model considered. It contains the noise components in the denominator of the complete noise model (Eq. 3.4), but disregards the second portion of the numerator, $4\frac{\langle MM^* \rangle}{\langle A^2 \rangle}$. This variant model, (Eq. 3.5), will be utilized most frequently after the DSH model (Eq. 1.3) and applied to the data collected since an estimate of $\frac{\langle MM^* \rangle}{\langle A^2 \rangle}$ is difficult to obtain in our situation due to the unknown parameter needed for the second moment of the fish scattering amplitude random variable, $\langle A^2 \rangle$. Eq. 3.5 is based on our claim that the estimator is driven by the fourth normalized moment of the signal amplitude and that the second part of the numerator in Eq. 3.4, which may be difficult to obtain, is making a negligible contribution to the overall model when compared to the original numerator in the DSH model (Eq. 1.3). To understand the implications of this underlying assumption the numerator of Eq. 3.4 is discussed. Recall that the fish scattering amplitude, A , is composed of three random variables: the beam pattern modulation, the pulse envelope effects, and the fish scattering component. Acquiring the second moments of the beam pattern and pulse envelope distributions may be a challenge but can be done. However, given that the parameter describing the Rayleigh distributed amplitudes is determined to be the

mode, it can be seen in Appendix B that the normalized fourth moment of the amplitude, $\frac{\langle a^4 \rangle}{\langle a^2 \rangle^2}$, will equal two and the second moment will be twice the mode squared, i.e. $\langle a^2 \rangle = 2\sigma^2$ where σ is the mode. Thus, if four times the ratio of the expectation of the magnitude of the noise to the second moment of the amplitude is much less than the fourth normalized moment of the amplitude, i.e. $4\frac{\langle MM^* \rangle}{\langle A^2 \rangle} \ll \frac{\langle A^4 \rangle}{\langle A^2 \rangle^2}$, then the claim that the numerator of the estimator $\langle N \rangle$ is driven by the fourth normalized moment of the signal amplitude will hold true. However, knowing the estimate for the mode of the Rayleigh distribution is a possible challenge that may need to be addressed. In the simulations conducted to estimate the effects of the beam pattern contribution in this paper, the factor of $4\frac{\langle MM^* \rangle}{\langle A^2 \rangle}$ is much smaller than the fourth normalized moment of the amplitude for most values of SNR considered. As the noise levels increase the factor of $4\frac{\langle MM^* \rangle}{\langle A^2 \rangle}$ begins to dominate the estimate of $\langle N \rangle$. This result is verified by comparing a revised model,

$$\langle N \rangle = \left[\frac{\langle A^4 \rangle}{\langle A^2 \rangle^2} + 4\frac{\langle MM^* \rangle}{\langle A^2 \rangle} \right] \left[\frac{\langle I^2 \rangle}{\langle I \rangle^2} - 2 \right]^{-1}, \quad (3.6)$$

of the DSH-N model (Eq. 3.4), with Eq. (1.3). The model defined by Eq. (3.6) has been modified from the DSH-N model (Eq. 3.4) by removing the moments of the noise contributions in the denominator. Comparisons between all models will be discussed in detail later on.

Due to a restricted number of iterations in empirical estimations and a limited amount of data collected, there will be an associated error in the scintillating index of the intensity in both the simulations conducted and the data analysis. This variance in SI (which results in an estimated error of $\langle N \rangle$ and ρ) can be empirically estimated for the simulations and data and then compared to expected errors found from an analytical form. Denbigh *et. al.* (1991) [11] derived an expression for the $Var(SI)$:

$$Var\left(\frac{\langle I^2 \rangle}{\langle I \rangle^2}\right) = \frac{\left[\frac{\langle I^4 \rangle}{\langle I \rangle^4} - 4 \left(\frac{\langle I^3 \rangle}{\langle I \rangle^3} \right) \left(\frac{\langle I^2 \rangle}{\langle I \rangle^2} \right) + 4 \left(\left(\frac{\langle I^2 \rangle}{\langle I \rangle^2} \right)^3 - \left(\frac{\langle I^2 \rangle}{\langle I \rangle^2} \right)^2 \right)^2 \right]}{n}, \quad (3.7)$$

where n is the number of independent samples taken. If the fourth normalized moment of the pulse envelope is equal to one an estimate of $Var(\langle N \rangle)$:

$$Var(\langle N \rangle) = \langle N \rangle^2 Var\left(\frac{\langle I^2 \rangle}{\langle I \rangle^2}\right)^{1/2} \left[\frac{\langle a^4 \rangle}{\langle a^2 \rangle^2} \frac{\langle b^4 \rangle}{\langle b^2 \rangle^2} \right]^{-1} \quad (3.8)$$

can be found in Denbigh *et. al.* (1991) [11]. New formulations of $Var(\langle N \rangle)$ are made for the variant model (Eq. 3.5) to include noise contributions and can be seen in Appendix C. For all four models in the simulations, variance estimates of the average number of fish per resolution cell are found by creating a number of ensembles for each SNR value, each containing a set of samples, and then estimated across the ensembles. Along these same lines, variance estimates of SI and $\langle N \rangle$ in the data are found by applying a bootstrapping method. Since the data set is comprised of

a small number of samples, an estimate for the variance in $\langle N \rangle$ can be made by resampling the small data set, a process also known as bootstrapping [12]. The results from these experiments are presented below and can be seen in Figure 4.

In the simulations conducted, estimates of the average number of fish are found for signal to noise ratios (SNR) between -40 dB and 60 dB as seen in Figure 4. As mentioned above, a variance estimate is empirically found at each SNR value for all four models and is used to measure the standard error in the $\langle N \rangle$ estimator. For signal to noise ratios of 20 dB or greater all four models accurately estimate the average number of fish per resolution cell with only small variations from the truth and a maximum (among all four models) margin of error of 0.94 fish per resolution cell. Our estimate of the margin of error is calculated by $1.96\sqrt{\frac{Var}{m}}$ where m is the sample size and is equal to 20. The estimate may not be normally distributed, but we still feel comfortable with this margin of error calculation. Around 20 dB the models began to diverge away from each other. As expected, the DSH-N model continues to vary slightly around the truth (with a margin of error ranging between 0.35 fish and 8 fish) for SNR down to -20 dB. The DSH model (Eq. 1.3) becomes increasingly inaccurate (standard deviations higher than 3.2 fish) for SNR of about 14 dB and lower; whereas the variant model (Eq. 3.5) continues to approximate small variations of the truth for signal to noise ratios as low as 9 dB with a maximum margin of error equaling 1.6 fish. Figure 5a and 5b illustrate the differences between all four models

considered. The variances of the estimates calculated from the true mean for each noise level are determined for all the models considered and are presented in Figure 5a. The variance estimates of $\langle N \rangle$ associated with the DSH model (Eq. 1.3) grow at a faster rate than the estimates for the variant model (Eq. 3.5) as the noise level increases. At approximately 17 dB, the rate of change in the variance estimates of (Eq. 1.3) increases by a factor of 5. However, (Eq. 3.5) doesn't experience such an increase until a signal to noise ratio of 11 dB has been reached thereby resulting in marginal improvements of the estimate of the average number of fish per resolution cell. This result confirms that, at least in this scenario, the numerator of the DSH-N model (Eq. 3.4) is primarily dominated by the fourth normalized moment of the signal amplitude, $\frac{\langle A^4 \rangle}{\langle A^2 \rangle^2}$, and the contribution of the second portion of the numerator, $4\frac{\langle MM^* \rangle}{\langle A^2 \rangle}$, is insignificant in comparison and can therefore be ignored. Thus, to avoid the complications of using the DSH-N model (Eq. 3.4), Eq. (3.5) may be a viable option to use for estimating fish number density along with the DSH calculation (Eq. 1.3). In order to calculate the average number of fish, $\langle N \rangle$, using Eq. (3.5), the first and second moments of the noise contributions, $\langle MM^* \rangle$ and $\langle (MM^*)^2 \rangle$, respectively, must be found and can be obtained by analyzing target-absent data. This may require user intervention and scrutinization of the data in practice. The differences between all four models can also be considered by viewing the absolute change of each from the true average for all noise levels. As seen in Figure 5b, at

approximately 14 dB, there is a 9% deviation from the truth in the DSH model (Eq. 1.3) that seems to increase as SNR decreases. However, the variant model (Eq. 3.5) differs from the truth by approximately 9% only when a signal to noise ratio of 10 dB has been reached. From this it appears that using the variant model, (Eq. 3.5), may result in less error at smaller SNR values than the DSH model, (Eq. 1.3). This may be attributed to the presence of the moments of noise, the differing assumption of the fish scattering statistic, or any combination of the differences implemented. Due to the difficulties of obtaining the parameter for the fish scattering statistic, only the DSH model (Eq. 1.3) and the variant model (Eq. 3.5) are considered when analyzing the example data collected.

CHAPTER 4

EXAMPLE WITH JUVENILE ATLANTIC BLUEFIN TUNA

The DSH model (Eq. 1.3) and the variant model derived (Eq. 3.5) are applied to a specific case of juvenile Atlantic Bluefin tuna fish schools (ABFT). We have reasonable information about the fish regarding their size and schooling tendencies and are therefore able to hypothesize about which distributions are more suitable to use for the components of the signal amplitude and phase. The use of a MBES allows us to obtain more complete pictures of the school shape due to the embedded directional capabilities and range resolution of the system as well as be able to quantify the limitations associated with it. The smallest hypothesized dimension of the fish length considered, at most 1.5 m, is much larger than the wavelength of the sonar system, ~ 0.0037 m. Also, the resonant frequency of the swim bladders of the fish explored, < 1 k Hz (Love 1978 and Nero 1996) [22, 26], is orders of magnitude smaller than the frequency used for transmission, 400 kHz. Together, these two aspects, along with a narrow beam, give us the ability to make fair assumptions and estimations of the needed pdfs for the resulting overall model and allow for confidence in the use of the DSH method (Eq. 1.3) and the variant method (Eq. 3.5) with a MBES.

4.1 Experiment Description

During the summer months of 2009 over the course of five days, ABFT fish schools were surveyed with both a MBES and aerial photography. The multibeam echosounder data and aerial imagery were being acquired simultaneously (Figure 6). The aircraft would direct the vessel towards the schools and photograph them (Figure 6a). As the vessel kept pace with the school, sonar imagery was collected from a sideways looking sonar mount on the side of the vessel (Figure 6b) during the time the aerial imagery was being acquired. The photographs from the flight provided a horizontal dimension of the fish school that could not be obtained from the sonar data. The fish schools imaged contained individuals estimated to be approximately 1.5 meters long with tendencies to stay about half a body length away from each other based on the observations made from the commercial spotter pilot and work done by Lutcavage [unpubl. date]. From the data collected, images where the vessel was not affecting the schools (more than 20 m from the fish) were analyzed in order to avoid the potential impacts on the shape of the school. To estimate fish number density using the previously mentioned models, sample sets of fish present data are considered where the main axis of the transmit and receive beams is thought to be within the school limits and not directed at a school edge. If the main response axis of a beam was pointed at the edge of the school the fluctuations in the signal would be attributed to the presence and absence of the fish which could contaminate

the results. The large differences between signals with fish and without fish would cause the scintillating index of intensity to converge to two and therefore impact the estimate of $\langle N \rangle$.

The modified assumptions of the DSH model (Eq. 1.3) are used when analyzing the data. As mentioned earlier, since the fourth normalized moment of a rectangular pulse is equal to one, the effects of the pulse envelope do not influence the estimate and can therefore be disregarded. Following the simulations, a Rayleigh distribution is chosen for the fish scattering statistic since the ratio of the fish length to wavelength is large. Thus the fourth normalized moment of the fish scattering distribution is equal to two. It is reasonable to assume, as in the DSH method, that the fish are uniformly located over some area and that the number of fish in a region of constant density is Poisson distributed. However, since the total area encompassing all fish locations at an average distance of 35 m from the boat is similar to the 11° by 11° hemi-ellipsoidal shell created in the simulations, the assumption of constant density within a hemispherical shell defined by an elevation angle of 90° is altered. The fourth normalized moment of the beam pattern is found using the same method as in the simulated data with the restricted area and is approximately equal to 40. The effects of the location of the beam within the school are also tested. As seen in Figure 7, the pdf of a beam centered in the middle of the school is similar to the distribution of a beam centered at the top of the school resulting in a fourth normalized moment

that differs only by a factor of 2. This is consistent with what is expected from using a narrow beam system. As mentioned earlier, the heavy peaks in the pdf are determined by the number of side lobes present. Regardless of where the narrow main lobe is located within the school, the number of side lobes encompassing the rest of the school will be large. Thus the directional changes in the main beam will not produce large inconsistencies in the estimate of $\langle N \rangle$ when using a narrow beam system. After all assumptions are incorporated into the model an estimate for fish number density can be found.

4.2 Estimate Fish Number Density

Estimating fish number density requires knowledge of the average number of fish per resolution cell, $\langle N \rangle$, and the volume of the area being ensonified. The volume found by using the 11° by 11° hemi-ellipsoidal shell is estimated using the volume of a spherical cap shell with an elevation angle of 5.5° and is approximately equal to 9.88 m^3 . In order to find the average number of fish per resolution cell, $\langle N \rangle$, for the juvenile Atlantic Bluefin Tuna data collected, a series of consecutive sonar images (124 pings) containing fish are analyzed from August 16, 2009. For a given beam and sample number (defined as the resolution cell) a scintillating index of intensity, $SI = \frac{\langle I^2 \rangle}{\langle I \rangle^2}$, is calculated for the time series. Contributions to the signal other than actual fish targets are considered noise contributions. Since a threshold has not been imposed on the data, certain signal reflectors different from the fish targets are still

present within the image such as multipath reflections (the image school created by reflections from the surface). Influences from these noise contributions on the resulting estimate of fish number density will be discussed in depth later. Estimates of $\text{Var}(\langle N \rangle)$ are obtained by applying a bootstrapping technique to the data set. The number of bootstrap samples taken is 25. Figure 8a shows the raw second normalized moment of intensity for all resolution cells over a period of approximately 33 seconds with a ping rate of 0.27 seconds. In order to produce a smoothed estimate for the SI of intensity, a box car filter (moving average) was applied to the data. A box shaped pulse of 200 samples by 2 beams is convolved with the scintillating index of intensity to generate smoothed images as can be seen in Figure 8b. To better understand the physical interpretation of the SI of the intensity within the fish school, the image is transformed into cartesian coordinates of range and depth as seen in Figure 9. The black line indicates the hypothesized surface while the band of noise described by the horizontal blue band directly below the black line is attributed to electrical interference related to the construction of the sonar system. Due to the roll and heave of the vessel and the offset in depth of the transducer, there may be some variability in the placement of the surface. Since depth is positive, the “real” scintillating indices of the fish intensities (not from the multipath reflections) are within the positive range of depth. The simplest version of the boundary of the school can be determined by the smallest rectangle encompassing the school in

the beam and sample number space. From our estimation, this boundary can be determined by beams 115 to 126 and samples between 1221 and 2458 (the red box in Figure 8b). The small area of higher scintillating indices in Figure 8b, (i.e. beams between 129 and 142 and samples between 1540 and 1921), can be partially attributed to an artifact of the noise such as sea surface turbulence. Figure 10 is a compiled image of the scintillating index of the noise component, $\frac{\langle (MM^*)^2 \rangle}{\langle MM^* \rangle^2}$. This index is calculated over 124 pings of fish-absent data. Along with the electrical noise band found in Figure 10, a cluster of high-intensity patches are present within four meters above the hypothesized surface. This artifact may be due to surface reflections caused by the natural roughness of the surface. The presence of these surface intensities will conceivably affect the scintillating indices of the overall signal and cause them to be biased high as can be seen in Figure 8. However, since this band of surface intensities does not lie within the proposed fish school, it can be analyzed in depth at a later time. Thus, the average scintillating index of intensity for all cells considered as part of the school (i.e. beams between 115 and 126 and samples between 1221 and 2458) is approximately 20. The scintillating index is a normalized parameter and therefore has no units associated with it. It is important to note that the location of the beam within the school boundaries is irrelevant since there is a lack of differences in the observed scintillating indices of intensity across the school vertically.

From here, an average number of fish for a given resolution cell is calculated using both the DSH model (Eq. 1.3) and the variant model (Eq. 3.5). Recall that the fourth normalized moment of the fish scattering statistic is equal to two and the fourth normalized moment of the beam pattern statistic is equal to 79.47 for a beam whose main lobe is in the direction of the center of the school and has a maximum elevation angle of 5.5° . Figure 11a and 11b illustrate the estimates for both models using the smoothed data respectively. The moments of noise, $\langle (MM^*)^2 \rangle$ and $\langle MM^* \rangle^2$, used for the variant model (Eq. 3.5) are found from the fish-absent data collected on August 16, 2009. The mean estimate for the average number of fish in the DSH model is approximately equal to 9.01 fish per resolution cell differing from the variant model which produces approximately 7.04 fish per resolution cell within the school (i.e. beams between 115 and 126 and samples between 1221 and 2458). The average SNR value within the school is found to be approximately 13 dB. The difference in average number of fish per resolution cell between the two models seems comparable to the results found when comparing the difference in the models from the simulated data. At 13 dB the DSH model (Eq. 1.3) and the variant model (Eq. 3.5) differ by 1.97 fish per resolution cell. After applying a bootstrapping technique to the observed data, estimates of the variance in $\langle N \rangle$ are obtained. As seen in Figure 11a, the estimates of the DSH formulation along the edges of the school are extremely variable and have associated standard deviations reaching

up to values of 20 or more fish per resolution cell. However, within the school, the estimates appear to be more accurately estimating the average number of fish with small standard deviations ranging between 0 and 15 fish per resolution cell. In Figure 11b, the edges of the school derived found from the variant model, (Eq. 3.5), appear to be less variable (by two orders of magnitude) than the DSH model and the artifact discussed above that is found in the noise is accounted for more accurately in the variant model. Within the school standard deviations range between 0 and 5 fish per resolution cell for the variant model. To better understand the differences between the two models, the ratio of variances is considered in Figure 12 (i.e. $Var(\langle N \rangle_{Eq.3.5})/Var(\langle N \rangle_{Eq.1.3})$). Resolution cells where the ratio is less than or equal to one help indicate that the variant model, (Eq. 3.5), is estimating the average number of fish with less variability than the DSH model, (Eq. 1.3). Inside the bounds of the school, (i.e. beams between 115 and 126 and samples between 1221 and 2458), the average of the ratios is approximately equal to 0.3. To verify that the results from both methods are accurately estimating the average number of fish per resolution cell, outside of considering the variance of the estimates, the fish number density is found and compared to the expected average number of fish (in the school) determined by the observations made by the aircraft pilot.

Found from both the aerial and multibeam data collected, the shape of the observed fish school can be modeled by an ellipsoid with dimensions of 31 m for the

major axis, 13 m for the minor axis, and 9 m for the vertical axis, as described in Weber *et. al.* [2012] [43]. Thus producing a total volume of 1899 m³ for the entire fish school. From the aerial imagery, the maximum total number of individual fish counted in Weber *et. al.* [2012] [43] is equal to 263 fish. Since this estimate of the total number of fish is derived from the photographs which collapse the image of the school onto a two-dimensional plane and do not account for individuals being hidden by the surface layer of fish and the maximum depth the school may have, the true total number of fish is expected to be larger than this estimate. In determining fish number density using the methods outlined in this paper, the estimates of $\langle N \rangle$ for each resolution cell are normalized by the 11° by 11° hemi-ellipsoidal shell volume (9.88 m³) producing average densities approximately equal to 0.91 fish/m³ for the DSH model (Eq. 1.3) and 0.71 fish/m³ for the variant model (Eq. 3.5). Given the volume of the whole school, 1899 m³, the resulting estimate for the average number of fish in the school would approximately be 1732 and 1353 fish for the DSH model and the variant model respectively. Both models vary, by more than a factor of 5, from the hypothesized estimate for the total number of fish (263 fish). This could be a byproduct of a few issues that have not been thoroughly addressed as well as incorrect assumptions made.

The current estimate for the number of fish per resolution cell, $\langle N \rangle$, and consequently the fish number density, ρ , does not account for possible multipath

effects. It is plausible that due to the geometry of the experiment conducted, false targets that appear above the surface can be included in the backscattered signal. If the image school that appears above the surface is making a significant contribution to the resulting estimates, every fish may appear to have multiple copies of itself that will increase the estimate and thus need to be accounted for. A single fish could be counted multiple times a number of ways in one pulse. However, considering the setup of the experiment, there are four paths that are of particular interest to us (Figure 13). As seen in Figure 13a and 13b, a fish below the surface could appear on the direct path as well as the path that hits the surface first and then scatters off of the fish back towards the sonar. Along with this, the partner image fish would have two associated paths: 1) a path to the fish then to the surface and back to the sonar, and 2) a path to the surface then to the fish then again back to the surface and finally back to the sonar as seen in Figure 13c and 13d, respectively. Therefore, every fish within the hypothesized school may have an intensity value four times higher than the true value. To adjust for this bias the estimate of $\langle N \rangle$ can be divided by four. However, the fourth normalized moment of the beam pattern also needs to be reconsidered. If there are multipaths and the image school is influencing the estimate, the beam pattern elevation angle needs to be widened so that the image school is included within the volume of ensonification. To include these changes, a first order estimate of $\langle N \rangle$ can be made by doubling the volume and recalculating

the fourth normalized moment of the beam pattern over a wider range of angles. The main response axis of the beam is still centered towards the middle of the real school while the elevation angle in one direction is increased to include the image school. The modified estimate of the fourth normalized moment of the beam pattern is equal to 302.98. This change, along with the doubled volume and the increased number of multipaths, results in a modified estimate of $\langle N \rangle$ equaling 34.45 and 26.83 fish per resolution cell for the DSH model (Eq. 1.3) and the variant model (Eq. 3.5) respectively. From here the fish number density for the DSH method is found to be 0.44 fish/m³ reflecting a total number of fish in the school to be 825.49 on average. The fish number density for the variant method is equal to 0.34 fish/m³ implying that, on average, the total number of fish within the school is 644.81. Although both estimates now appear to be much more plausible given the hypothesized number of fish within the school, both are still off by at least a factor of 2. Another source of error that can somewhat be accounted for in the simulation is the assumption of the beam pattern calculation.

Although the Mills Cross setup appears to be the most accurate setup for simulating a multibeam system in this situation, knowing and implementing the actual beam pattern and side lobe levels used in the experiment can be difficult. The estimates for the fourth normalized moment of the beam pattern have been found with a Mills Cross array setup defined by Chebyshev windows with side lobe levels of 30

dB. In other circumstances this choice for the simulation of the sonar system may be accurate, however after further analysis the Reson 7125 multibeam sonar system used for the experiment can be better represented with side lobe levels of 20 dB (Lanzoni and Weber 2010) [21]. With this change, the fourth normalized moment of the beam pattern becomes 230.49 and the estimate for the average number of fish per resolution cell changes to 26.13 for the DSH method and 20.4 for the variant method. This will result in a fish number density for the DSH method of 0.33 fish/m³ and 627.98 fish in the entire school. For the variant model, the fish number density is equal to 0.26 fish/m³ and 490.53 fish within the school. Although both estimates appear to be biased high relative to the hypothesized true number of fish (263 fish), the observed number is known to be biased low due to the projection of the school onto a two dimensional plane. There may also be other unknown sources of error within the assumptions and/or the estimates.

CHAPTER 5

DISCUSSION

Estimating fish number density using traditional techniques can be difficult due to the limitations and uncertainties associated with such methods. First, calibrating the system used can prove to be tedious, costly and time consuming. Second, measuring target strength values can be challenging and the uncertainty associated with the values remains a significant source of error in estimating number density (Simmonds and McLennan 2005).

The DSH model developed is a useful tool that can help mitigate the disadvantages of traditional techniques. Since the model is based on normalized moments, calibrated backscatter measurements are un-necessary as they would cancel out in the formulation of the scintillating index of intensity. Also, estimates of target strength do not need to be made in order to implement this model. The assumptions and components of the DSH model, however, may need to be reviewed depending on the situation. The only information required describing the fish being considered are the distribution of scatterer amplitudes and the spatial distribution of the fish, determined by regions of density and areas of ensonification. Such assumptions will greatly affect the outcome

of the fish scattering statistic and beam pattern fluctuation and thus the resulting signal amplitude as well as the phase of the contributors. The Rayleigh assumption of the amplitude scattering hasn't been discussed deeply and can be difficult to test, but can easily be altered with the use of this model if needed as long as the statistics stay out of the Gaussian limit. The assumptions made about uniform density within a volume should be carefully examined when the tendencies of the observed school are to cluster in certain areas and the model used should be modified to include the possible effects. The volume being ensonified will greatly affect the estimate of fish number density when using the DSH model. As discussed earlier and seen in Figure 2, the ratio of the fourth normalized moment of the beam pattern to the area of coverage will have larger associated error with small volumes of ensonification than with larger volumes. Close proximity to the school can help alleviate this issue.

Although many of the DSH assumptions can be modified to the situation at hand, in order to obtain accurate estimates of $\langle N \rangle$ and find the model requires a low number of fish to be ensonified, or equivalently a scintillating index much greater than two. The effects of scintillating indices close to two can possibly be addressed by using a different transducer and modifying the assumptions of the model. The noise contribution may be an important aspect to consider as well. If the sonar system used and the environment being worked in produce signal to noise ratio's greater than 20 dB then the DSH model will produce an accurate estimate of fish

number density with a calculated maximum margin of error equal to 0.94 fish per resolution cell. However, as mentioned earlier, as the noise levels increase the model diverges from the true estimate at a fast rate (Figure 4). This can be expected since the estimator is inherently noisy incorporating higher order moments derived from heavily peaked distributions. The effects of these normalized higher order moments on the estimate of $\langle N \rangle$ can be tempered with the use of a narrow beam system as well as the ensonification of a low number of fish. The use of a MBES can help achieve this small number density as well as provide adequate range resolution and directionality.

In order to improve upon the estimates of the DSH model for high noise situations, a version of a modified noise model (Eq. 3.5) can be implemented. Although the use of the complete noise model (Eq. 3.4) would achieve the best estimates for all noise levels, the difficulty in obtaining the information needed could negate the benefits of the DSH model. The DSH model (Eq. 1.3), the complete noise model referred to as the DSH-N model (Eq. 3.4), and two variations of the noise model (Eq. 3.5 and Eq. 3.6), were simulated here in order to determine the most suitable method to use in the circumstances presented. Since the information needed for the complete noise model would be difficult to obtain here, the variant model (Eq. 3.5), and the DSH model (Eq. 1.3), were chosen to use with observed juvenile Atlantic Bluefin Tuna data. For a sample set of pings collected on August 16, 2009, the estimates of fish

number density were calculated for both models and compared with the observations made from the aerial imagery obtained simultaneously. Although there were observed differences between the hypothesized number of fish within the school and the original estimates made using the DSH method and the variant method, there are promising results when certain assumptions are modified and various parameters accounted for. As seen in the results, multipath reflections make a significant impact on the estimates made. Extending the volume of interest to include the mirror school may change the assumption that the fish are uniformly distributed since there will be some volume between the image school and the real school that is absent of fish but is still used in the calculation. Knowing the details of the beam pattern of the sonar system used are very important as seen in the work done here. Difficulties may come from trying to simulate the sonar and not knowing true side lobe levels or which window functions to use. Understanding the implications of the beam location within the school could also be an important parameter to account for since the fourth normalized moment can be significantly different for a beam directed towards the middle of the school versus a beam in the direction of the boundary of the school. The assumption of the fish scattering statistic may need to be reconsidered as well. It is possible that multiple contributions may be coming from one fish due to the orientation and curvature of its body within the ensonified volume, thus the assumption that a scatterer is one fish may need to be addressed. Also, since the school has changed location

and orientation in every ping, assuming the school shape is approximately ellipsoidal every time may be an issue to consider. Another obstacle that cannot be addressed is knowing the exact number of fish. Even though the hypothesized true number of fish may be somewhat accurate, it will be biased low due to the projection onto a two dimensional plane. Although the estimates found here are on the same order of magnitude as the hypothesized average number of fish within the school, it is possible that there are a number of other unknown parameters that have not been accounted for here. However, our promising results suggest that the use of the DSH model and the variant model in estimating fish number density with backscattered pressure signals prove to be very successful.

CHAPTER 6

FIGURES

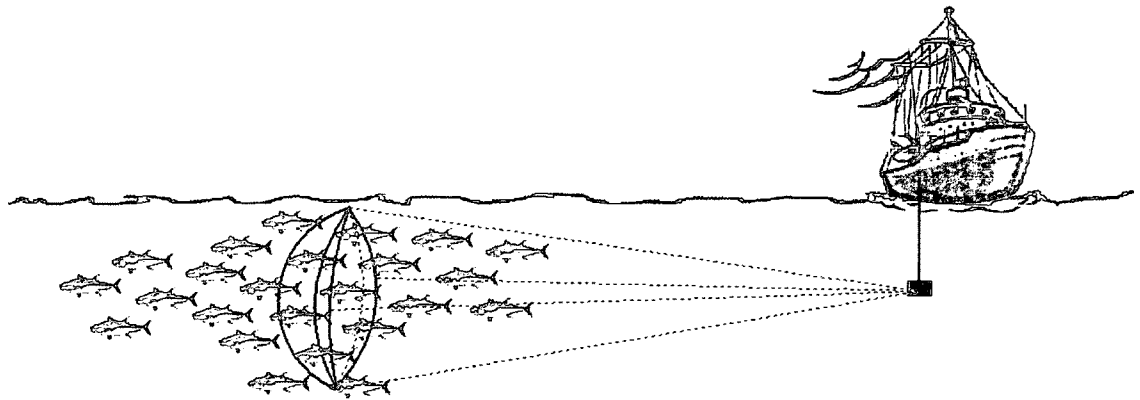


Figure 6-1. Environmental setup for the simulations conducted and data analyzed. The number of contributors for a given resolution cell are determined by the hemi-ellipsoidal shell encompassing the school at some range r with a thickness determined from the pulse length, τ , and sound speed, c . On average, the shell can be approximated by an 11° by 11° hemi-ellipsoidal shell.

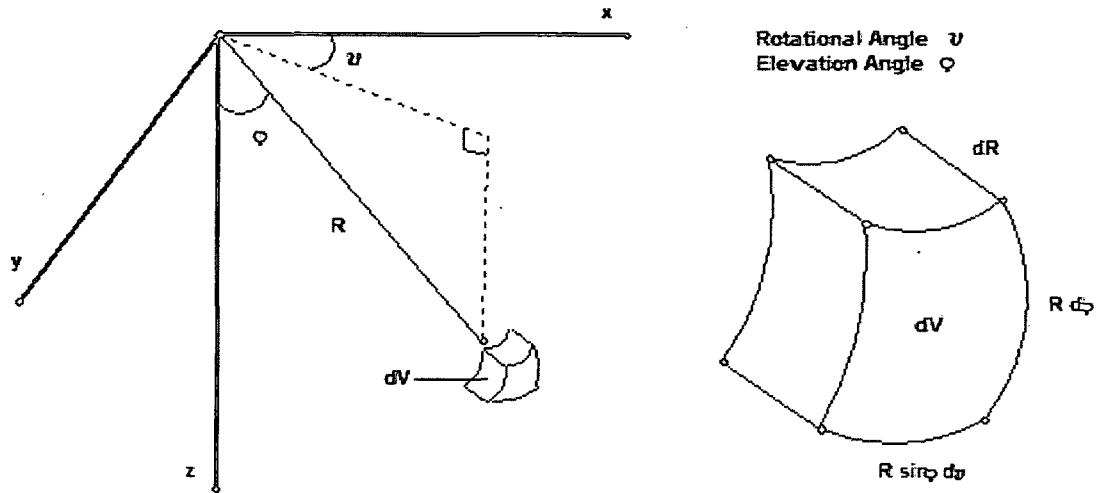


Figure 6-2. Geometry of the backscattering measurements. The change in volume is represented by $dV = R^2 \sin(\phi) dR d\phi d\nu$ where ϕ is the elevation angle and ν is the rotational angle.

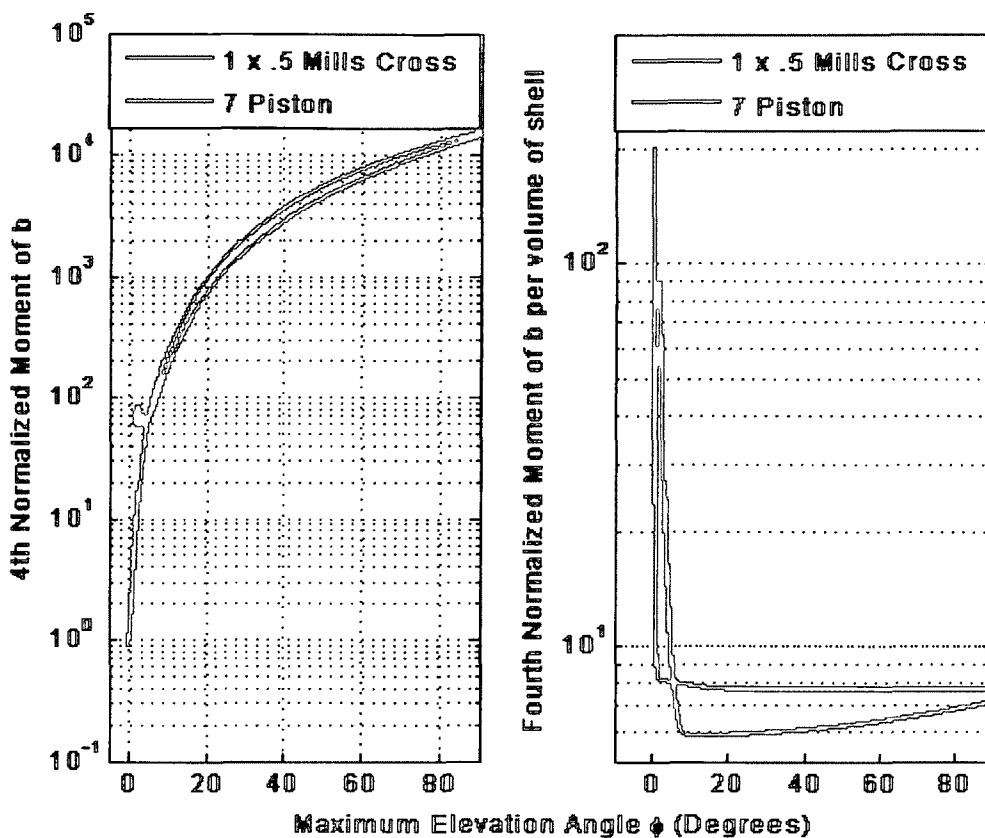


Figure 6-3. (a) Change in fourth normalized moment of $b(\nu, \phi)$ for varying elevation angles (ϕ). (b) Ratio of the fourth normalized moment of $b(\nu, \phi)$ to volume for varying elevation angles. The blue curves represent the Mills Cross 1° by 0.5° transducer and the red curves represent the 7° transducer. For small elevation angles in (a), numerical error arises.

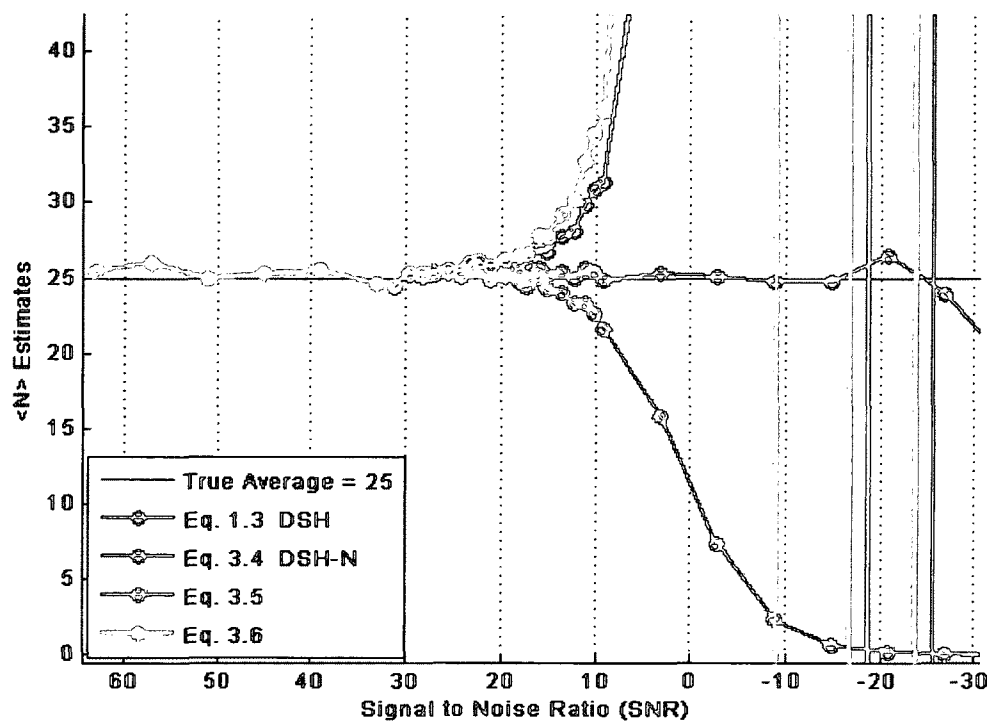


Figure 6-4. Estimates of the average number of fish per resolution cell, $\langle N \rangle$. A Mills Cross 1° by 0.5° transducer is simulated with an elevation angle, ϕ , equal to 5.5° . The true estimate of $\langle N \rangle$ is equal to 25 fish per resolution cell.

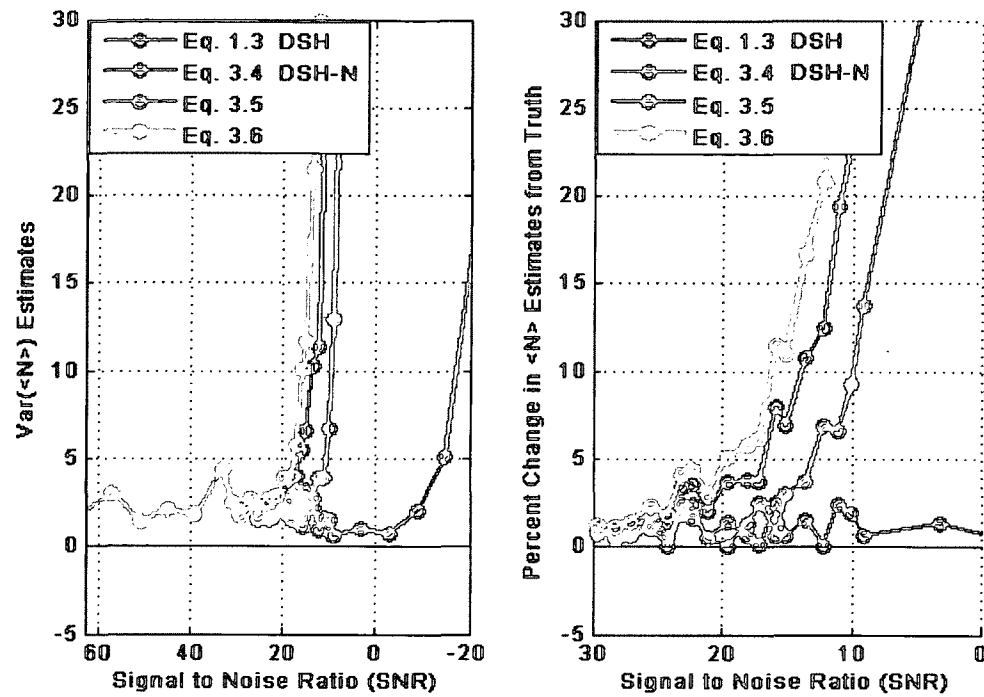


Figure 6-5. Error estimates in $\langle N \rangle$. (a) Variance of $\langle N \rangle$. (b) Absolute percent change in $\langle N \rangle$ from the true value.

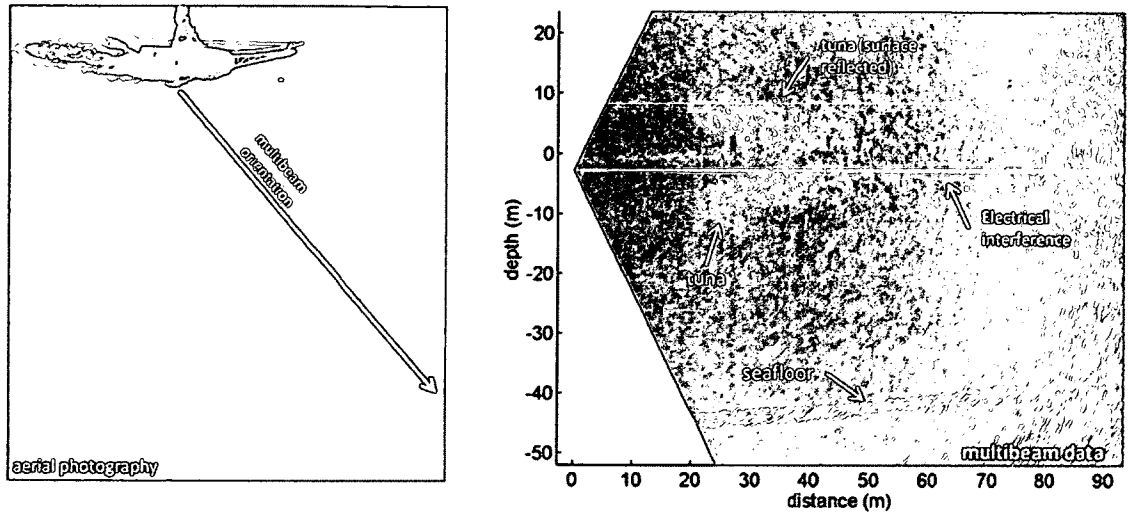


Figure 6-6. Experimental setup for the data collected. (a) Aerial image of the ABFT school with the side-looking 400 kHz MBES. (b) A single ping from the multibeam showing a vertical cross-section of the school.

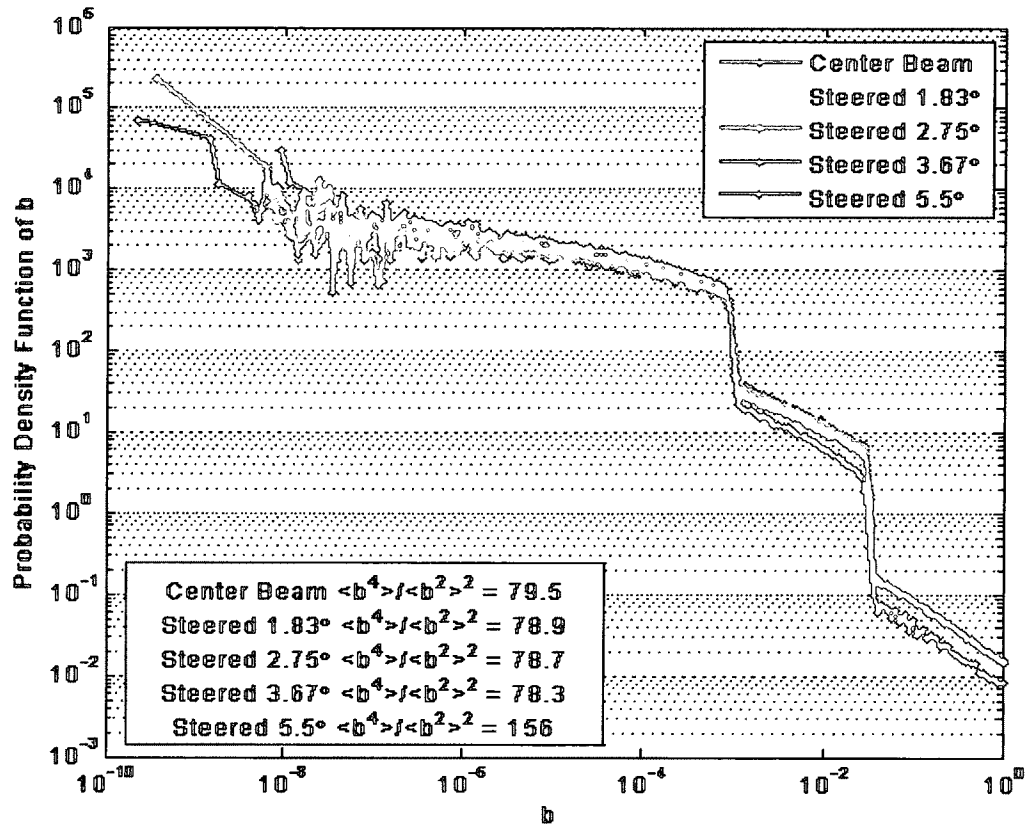


Figure 6-7. Probability Density Function of $b(\nu, \phi)$ from a Mills Cross 1° by 0.5° transducer. The rotational angle, ν , ranges from 0 to 360° . The elevation angle, ϕ , is restricted between 0 and 5.5° . A centered beam (red line), a 1.83° steered beam (yellow line), a 2.75° steered beam (green line), a 3.67° steered beam (magenta line), and a 5.5° steered beam (blue line) are simulated. The fourth normalized moments of each beam are represented.

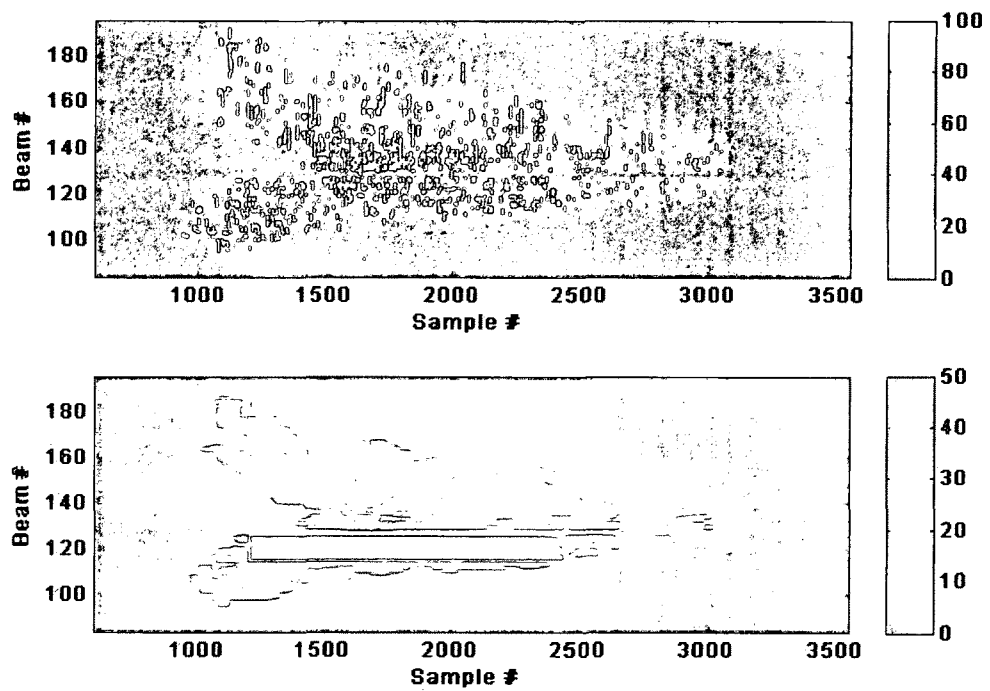


Figure 6-8. Scintillating index of intensity (SI) over 124 pings. (a) Raw estimates of SI. (b) Smoothed estimates of SI with a box car filter over 100 samples and 2 beams. SI is a unitless parameter. The red box represents the boundary of the fish school.

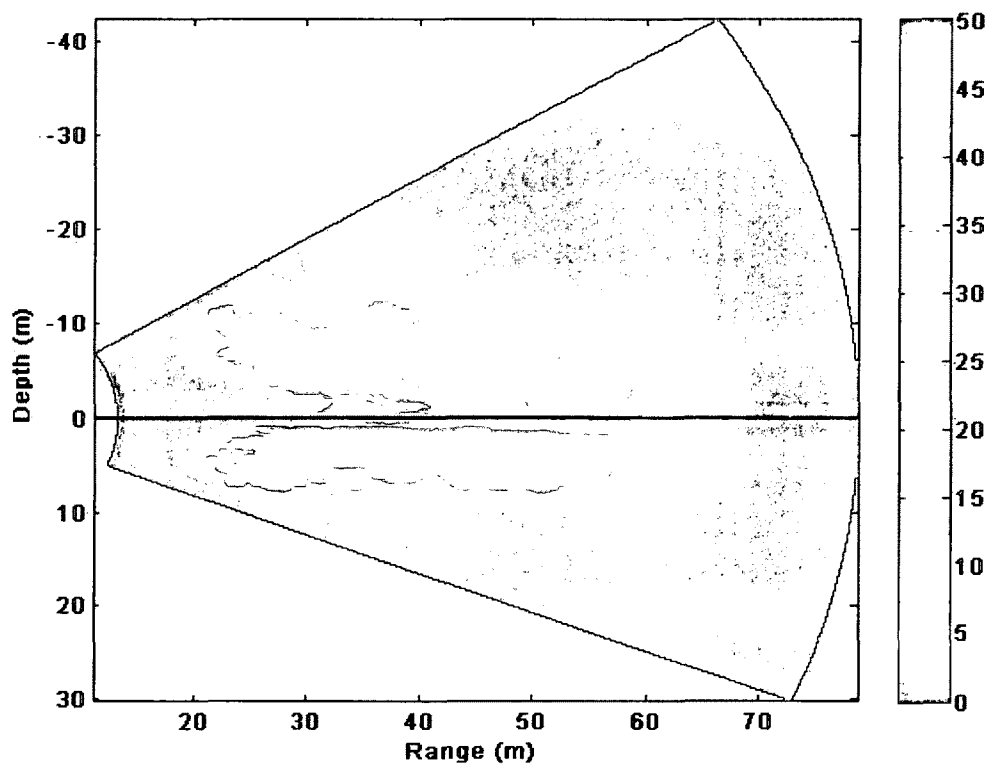


Figure 6-9. Smoothed scintillating index of intensity represented in cartesian coordinates (over 124 pings). The hypothesized surface is represented by the horizontal black line.

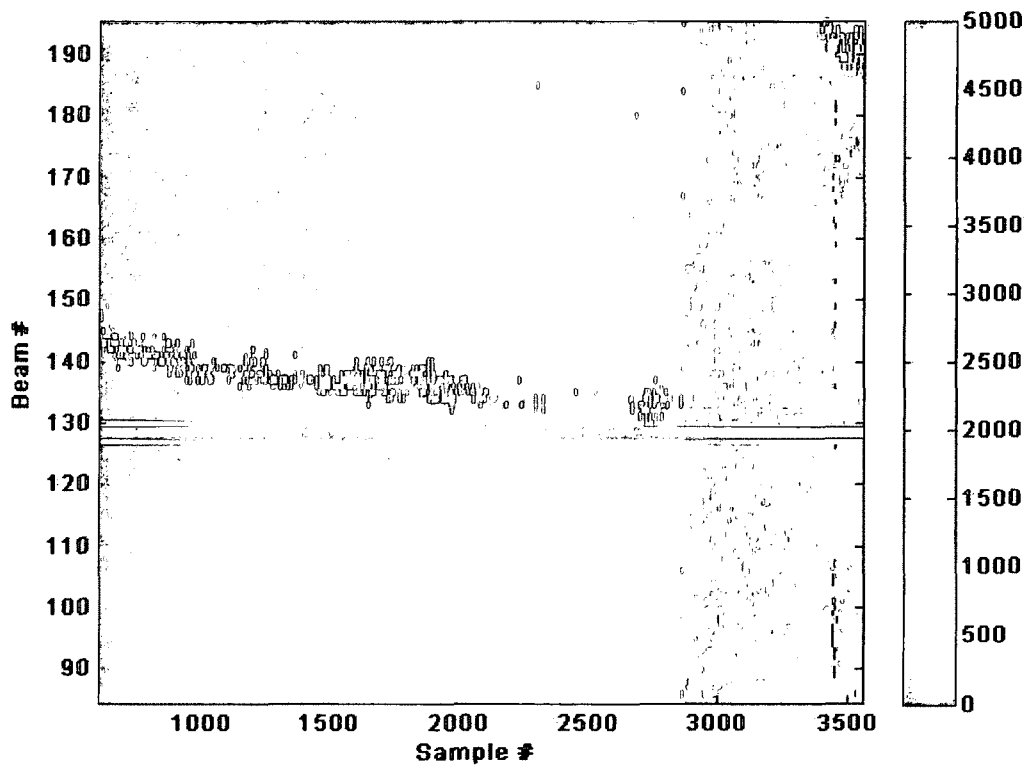


Figure 6-10. Unsmoothed scintilating index of the noise contribution, $\frac{\langle (MM^*)^2 \rangle}{\langle MM^* \rangle^2}$, found over 124 pings of target-absent data.

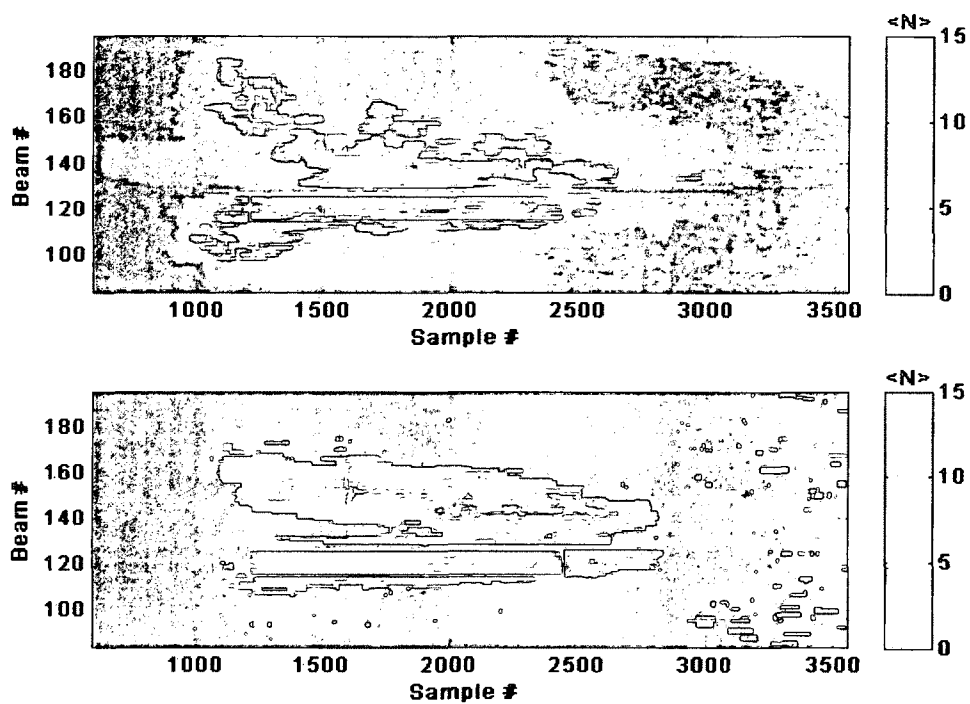


Figure 6-11. (a) $\langle N \rangle$ estimate from the DSH model (Eq. 1.3). (b) $\langle N \rangle$ estimate from the variant model (Eq. 3.5). Both are found over a smoothed SI. The red box represents the boundary of the fish school. Units of $\langle N \rangle$ are in fish per resolution cell.

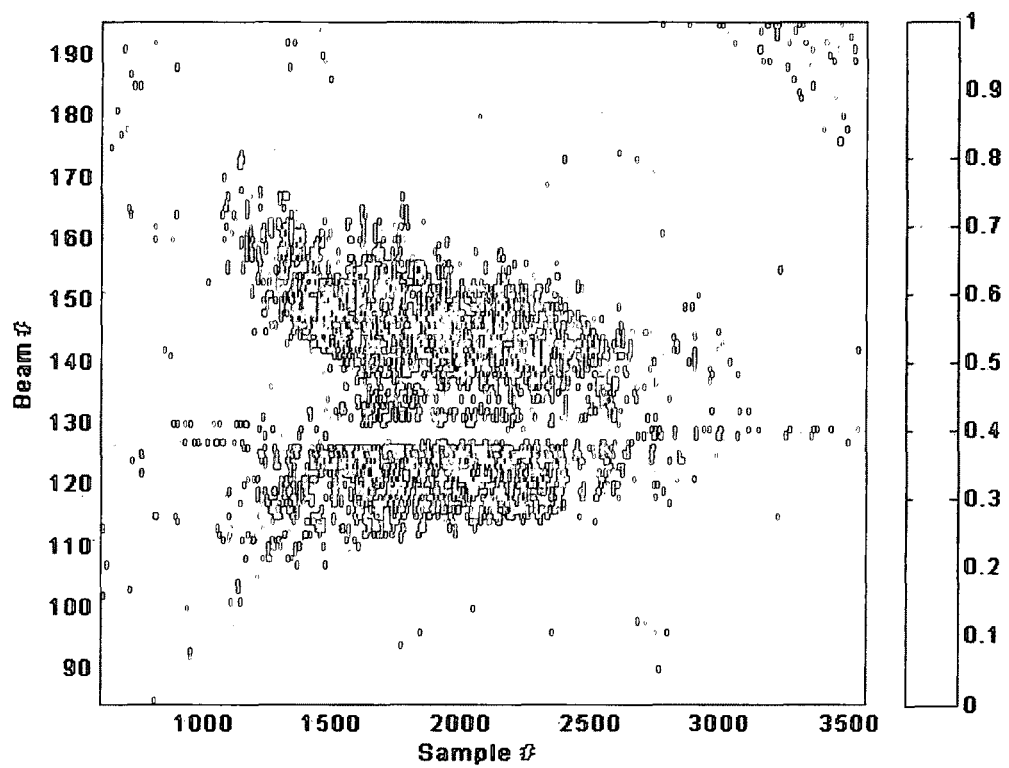


Figure 6-12. Ratio of the variance of the variant model (Eq. 3.5) to the variance of the DSH model (Eq. 1.3), i.e. $Var(\langle N \rangle_{Eq.3.5})/Var(\langle N \rangle_{Eq.1.3})$.

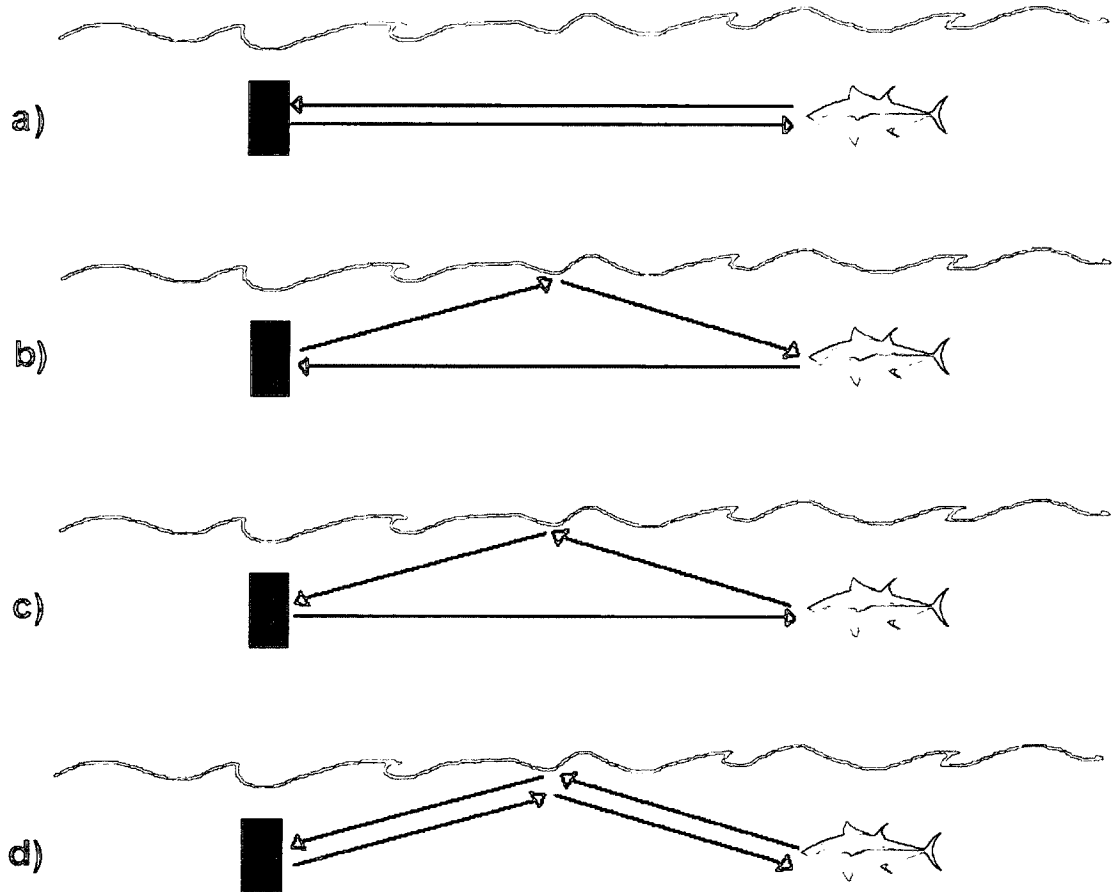


Figure 6-13. Multiple sound paths between the sonar and fish. (a) Direct path. (b) Reflection from the surface to the fish and back to the sonar. (c) Reflection from the fish to the surface and back to the sonar. (d) Reflection to the surface, then the fish, back to surface, with a return to the sonar.

BIBLIOGRAPHY

- [1] D.A. Abraham and A.P. Lyons. Novel physical interpretations of k-distributed reverberation. *IEEE Journal of Oceanic Engineering*, 27:800–813, 2002.
- [2] V. Bluemel, L.M. Narducci, and R.A. Tuft. Photon-count distributions and irradiance fluctuations of a log-normally distributed light field. *Journal of Optical Society of America*, 62(11):1309–1314, 1974.
- [3] P. Brehmer, T. Lafont, S. Georgakarakos, E. Josse, F. Gerlotto, and C. Collet. Omnidirectional multibeam sonar monitoring: applications in fisheries science. *Fish and Fisheries*, 7:165–179, 2006.
- [4] E.L. Cadima. *Fish stock assessment manual*. FAO, 2003.
- [5] D. Chu and T.K. Stanton. Statistics of echoes from a directional sonar beam insonifying finite numbers of single scatterers and patches of scatterers. *IEEE Journal of Oceanic Engineering*, 35:267–277, 2010.
- [6] C. Clay and H. Medwin. *Acoustical Oceanography: Principles and Applications*. John Wiley and Sons, New York, USA, 1977.
- [7] C.S. Clay and B.G. Heist. Acoustic scattering by fish–acoustic models and a two-parameter fit. *Journal of Acoustical Society of America*, 75(4):1077–1083, 1984.
- [8] N.A. Cochrane, Y. Li, and G.D. Melvin. Quantification of a multibeam sonar for fisheries assessment applications. *Journal of Acoustical Society of America*, 114:745–758, 2003.
- [9] A.B. Cooper, University of New Hampshire. Sea Grant Program, National Sea Grant College Program (U.S.), United States. National Oceanic, and Atmospheric Administration. *A guide to fisheries stock assessment: from data to recommendations*. University of New Hampshire, Sea Grant College Program, 2006.

- [10] G.R. Jr Cutter and D.A. Demer. Accounting for scattering directivity and fish behaviour in multibeam-echosounder surveys. *ICES Journal of Marine Science*, 64:1664–1674, 2007.
- [11] P. Denbigh, Q. Smith, and I. Hampton. Determination of fish number density by a statistical analysis of backscattered sound. *Journal of Acoustical Society of America*, 90(1):457–469, 1991.
- [12] B. Efron and R.J. Tibshirani. *An Introduction to the Bootstrap*. Chapman and Hall/CRC, Boca Raton, FL, first edition, 1993.
- [13] J.E. Ehrenberg. A method for extracting the fish target strength distribution from acoustic echoes. In *Proceedings IEEE Conference Engineering in the Ocean Environment*, volume 1, pages 61–64, 1972.
- [14] J.E. Ehrenberg. Mathematical model for volume reverberation: experiment and simulation. *Journal of Acoustical Society of America*, 55(2):227–236, 1974.
- [15] P.G. Fernandes, F. Gerlotto, D.V. Holliday, O. Nakken, and E.J. Simmonds. Acoustic applications in fisheries science: the ices contribution. *ICES Marine Science Symposia*, 215:483–492, 2002.
- [16] K.G. Foote. Fish target strengths for use in echo integrator surveys. *Journal of Acoustical Society of America*, 82:981–987, 1987.
- [17] F. Gerlotto, S. Georgakarakos, and P.K. Eriksen. The application of multibeam sonar technology for quantitative estimates of fish density in shallow water acoustic surveys. *Aquatic Living Resources*, 13:385–393, 2000.
- [18] F. Gerlotto and J. Paramo. The three-dimensional morphology and internal structure of clupeid schools as observed using vertical scanning multibeam sonar. *Aquatic Living Resources*, 16:113–122, 2003.
- [19] F. Gerlotto, M. Soria, and P. Freon. From two dimensions to three: the use of multibeam sonar for a new approach in fisheries acoustics. *Canadian Journal of Fisheries and Aquatic Sciences*, 56:6–12, 1999.
- [20] C.W.D. Gurshin, J.M. Jech, H. Howell, T.C. Weber, and L.A. Mayer. Measurements of acoustic backscatter and density of captive atlantic cod with synchronized 300-khz multibeam and 120-khz split-beam echosounders. *ICES Journal of Marine Science*, 66:1303–1309, 2009.
- [21] J.C. Lanzoni and T.C. Weber. High-resolution calibration of a multibeam echo sounder. In *Proceedings MTS/IEEE Oceans 2010 Conference*, 2010.

- [22] R.H. Love. Resonant acoustic scattering by swimbladder-bearing fish. *Journal of Acoustical Society of America*, 64(2):571–580, 1978.
- [23] J.B. Lozow. Transducer directivity: A simple calculation of its spatial averages. In J.B. Suomala, editor, *Meeting on Hydroacoustical Methods for the Estimation of Marine Fish Populations. 25-29 July 1979. II: Contributed Papers, Discussion and Comments*, Charles Stark Draper Laboratory, Cambridge, MA, 1981.
- [24] A.P. Lyons and D.A. Abraham. Statistical characterization of high-frequency shallow-water seafloor backscatter. *Journal of Acoustical Society of America*, 106:1307–1315, 1999.
- [25] L. Mayer, J.H. Clarke, and S. Dijkstra. Multibeam sonar: potential applications for fisheries research. *Journal of Shellfish Research*, 17(5):1463–1467, 1999.
- [26] R.W. Nero. Model estimates of acoustic scattering from schools of large yellowfin tuna. Technical Report NRL/MR/7174-95-7708, Naval Research Laboratory, Stennis Space Center, MS, 1996.
- [27] K. Patterson, R. Cook, C. Darby, S. Gavaris, L. Kell, P. Lewy, B. Mesnil, A. Punt, V. Restrepo, D.W. Skagen, and G. Stefansson. Estimating uncertainty in fish stock assessment and forecasting. *Fish and Fisheries*, 2(2):125–157, 2001.
- [28] M.L. Peterson, C.S. Clay, and S.B. Brandt. Acoustic estimates of fish density and scattering function. *Journal of Acoustical Society of America*, 60(3):618–622, 1976.
- [29] A.D. Pierce. *Acoustics: An introduction to its principles and applications*. Acoustical Society of America, Melville, NY, 1 edition, 1981.
- [30] E.K. Pikitch, C. Santora, E.A. Babcock, A. Bakun, R. Bonfil, D.O. Conover, P. Dayton, P. Doukakis, D. Fluharty, B. Heneman, E.D. Houde, J. Link, P.A. Livingston, M. Mangel, M.K. McAllister, J. Pope, and K.J. Sainsbury. Ecosystem-based fishery management. *Science*, 305:346–347, 2004.
- [31] P.N. Pusey, D.W. Schaefer, and D.E. Koppel. Single-interval statistics of light scattered by identical independent scatterers. *Journal of Physics A: Mathematical, Nuclear and General*, 7(4):530–540, 1974.
- [32] S.O. Rice. *Mathematical Analysis of Random Noise*. Bell System Technical Journal, New York, N.Y., 1945.
- [33] J. Simmonds and D. MacLennan. *Fisheries Acoustics: Theory and Practice*. Wiley-Blackwell, Oxford, UK, second edition, 2005.

- [34] M. Soria, T. Bahri, and F. Gerlotto. Effect of external factors (environment and survey vessel) on fish school characteristics observed by echosounder and multibeam sonar in the mediterranean sea. *Aquatic Living Resources*, 16:145–157, 2003.
- [35] R.C. Spindel and P.T. McElroy. Level and zero crossings in volume reverberation signals. *Journal of Acoustical Society of America*, 53(5):1417–1426, 1973.
- [36] S. Stanic and E.G. Kennedy. Reverberation fluctuations from a smooth seafloor. *IEEE Journal of Oceanic Engineering*, 18:95–99, 1993.
- [37] T.K. Stanton and D. Chu. Non-rayleigh echoes from resolved individuals and patches of resonant fish at 2-4 khz. *IEEE Journal of Oceanic Engineering*, 35:152–163, 2010.
- [38] T.K. Stanton and C.S. Clay. Sonar echo statistics as a remote-sensing tool: volume and seafloor. *IEEE Journal of Oceanic Engineering*, 11:79–96, 1986.
- [39] V.M. Trenkel, V. Mazauric, and L. Berger. The new fisheries multibeam echosounder me70: description and expected contribution to fisheries research. *ICES Journal of Marine Science*, 65:645–655, 2008.
- [40] R.J. Urick. *Principles of Underwater Sound*. McGraw-Hill, New York, 1983.
- [41] R.C. Waag, P.P.K. Lee, H.W. Persson, E.A. Schenk, and R. Gramiak. Frequency-dependent angle scattering of ultrasound by liver. *Journal of Acoustical Society of America*, 72(2):343–352, 1982.
- [42] R.K. Wallace and K.M. Fletcher. *Understanding Fisheries Management: A manual for understanding the Federal Fisheries Management Process, Including Analysis of the 1996 Sustainable Fisheries Act*. Mississippi-Alabama Seagrass Consortium, 2 edition, 2000.
- [43] T.C. Weber, M.E. Lutcavage, and M.L. Schroth-Miller. Near resonance acoustic scattering from organized schools of juvenile atlantic bluefin tuna (*Thunnus thynnus*). 2012.
- [44] T.C. Weber, H. Pena, and J.M. Jech. Consecutive acoustic observations of an atlantic herring school in the northwest atlantic. *ICES Journal of Marine Science*, 69:000–000, 2009.
- [45] P. Wilhelmij and P. Denbigh. A statistical approach to determining the number density of random scatterers from backscattered pulses. *Journal of Acoustical Society of America*, 76(6):1810–1818, 1984.

APPENDIX A

DERIVATION OF AVERAGE NUMBER OF FISH (PER RESOLUTION CELL)

1. New Pressure Model

In order to obtain the DSH model let M equal zero in the following derivation. Measuring pressure amplitudes:

$$P_M = \sum_{j=1}^N A_j e^{i\theta_j} + M$$

2. Model Assumptions

$$\begin{aligned} A_j &\sim \text{Rayleigh}(s) \\ \theta_j &\sim \text{Uniform}(0, 2\pi) \\ N &\sim \text{Poisson}(\lambda) \\ M &\sim \text{Complex Gaussian}, M = X + iY \text{ where } X, Y \sim N(\mu, \sigma) \end{aligned}$$

(a) Extended Notes on Model Assumptions

$$A \sim \text{Rayleigh} \implies \langle A \rangle = s\sqrt{\frac{\pi}{2}}, \langle A^2 \rangle = 2s^2, \langle A^4 \rangle = 8s^4$$

$$M = (X + iY) \sim \text{Complex Gaussian} \implies MM^* = X^2 + Y^2 \implies (MM^*)^2 = X^4 + 2X^2Y^2 + Y^4$$

$$X \sim \text{Normal} \implies \langle X \rangle = \mu, \langle X^2 \rangle = \mu^2 + \sigma^2, \langle X^4 \rangle = \mu^4 + 6\mu^2\sigma^2 + 3\sigma^4$$

So if $X, Y \sim N(\mu, \sigma)$, then $\langle MM^* \rangle = 2(\mu^2 + \sigma^2)$ and

$$\langle (MM^*)^2 \rangle = 2(\mu^4 + 6\mu^2\sigma^2 + 3\sigma^4) + 2(\mu^2 + \sigma^2)^2$$

3. Find Intensity I

$$I \approx |P_M^2| = P_M P_M^*$$

\Rightarrow

$$I = \left(\sum_{j=1}^N A_j e^{i\theta_j} + M \right) \left(\sum_{j=1}^N A_j e^{-i\theta_j} + M^* \right)$$

\Rightarrow

$$I = \sum_{j=1}^N \sum_{k=1}^N A_j A_k e^{i(\theta_j - \theta_k)} + M^* \sum_{j=1}^N A_j e^{i\theta_j} + M \sum_{j=1}^N A_j e^{-i\theta_j} + M M^*$$

4. Find the Expectation of Intensity $\langle I \rangle$

$$\begin{aligned} \langle I \rangle = & \langle \sum_{j=1}^N \sum_{k=1}^N A_j A_k e^{i(\theta_j - \theta_k)} \rangle + \langle M^* \rangle \langle \sum_{j=1}^N A_j e^{i\theta_j} \rangle \\ & + \langle M \rangle \langle \sum_{j=1}^N A_j e^{-i\theta_j} \rangle + \langle M M^* \rangle \end{aligned}$$

since the noise is independent of the signal

$$\begin{aligned} \text{Consider } E[\sum_{j=1}^N A_j e^{i\theta_j}] &= \sum_{j=1}^N E[A_j e^{i\theta_j}] \text{ since each are independent} \\ &= \sum_{j=1}^N E[A_j] E[e^{i\theta_j}] \text{ since } A_j \text{ is independent of } \theta_j \\ &= \sum_{j=1}^N E[A_j] \int_0^{2\pi} e^{i\theta_j} \frac{1}{2\pi} d\theta_j \text{ since } \theta_j \sim U(0, 2\pi) \\ &= \sum_{j=1}^N E[A_j] [-ie^{i\theta_j}]_0^{2\pi} = 0 \end{aligned}$$

So,

$$E[h e^{i\theta}] = 0 \text{ for any } h \text{ and } \theta \sim U(0, 2\pi) \text{ if } h \text{ and } \theta \text{ are independent} \quad (\text{A.1})$$

\Rightarrow

$$\langle I \rangle = \langle \sum_{j=1}^N A_j^2 + \sum_{j \neq k}^N A_j A_k e^{i(\theta_j - \theta_k)} \rangle + \langle M M^* \rangle$$

\Rightarrow

$$\langle I \rangle = \langle \sum_{j=1}^N A_j^2 \rangle + \langle M M^* \rangle$$

since $\langle \sum_{j \neq k}^N A_j A_k e^{i(\theta_j - \theta_k)} \rangle = 0$ by Eq. 1

Note $\langle \sum_{j=1}^N A_j^2 \rangle$ is Compound Poisson Random Variable, i.e. N and each A_j is a random variable.

So, $\langle I \rangle = \langle \langle I|N \rangle \rangle$

$$\begin{aligned} \langle I|N \rangle &= \langle \sum_{j=1}^n A_j^2 | N = n \rangle + \langle MM^* \rangle \\ &\quad \text{Wald's Identity: } N \text{ independent of } A_j \\ &= n \langle A_1^2 | N = n \rangle + \langle MM^* \rangle \\ &\quad \text{Each } A_j \text{ is iid and there are } n \text{ } A_j^2 \\ &= n \langle A_1^2 \rangle + \langle MM^* \rangle \\ &\quad A_1 \text{ doesn't depend on } n \end{aligned}$$

\Rightarrow

$$\langle \langle I|N \rangle \rangle = \sum_{n=1}^{\infty} \langle I|N \rangle P(N = n)$$

since n is discrete

$$= \langle N \rangle \langle A^2 \rangle + \langle MM^* \rangle$$

let A represent A_1 since all A_j are identically distributed

\Rightarrow

$$\boxed{\langle I \rangle = \langle N \rangle \langle A^2 \rangle + \langle MM^* \rangle}$$

5. Important Notes

(a) Note A

Recall,

$$\begin{aligned} \langle \sum_{j=1}^N A_j^2 \rangle &= \langle \sum_{j=1}^n A_j^2 | N = n \rangle \\ &= \langle N \rangle \langle A^2 \rangle \end{aligned}$$

(b) Note B

Consider,

$$\left\langle \left(\sum_{j=1}^N A_j^2 \right)^2 \right\rangle = \left\langle \sum_{j=1}^N A_j^4 \right\rangle + \left\langle \sum_{j \neq k}^N \sum_{j \neq k}^N A_j^2 A_k^2 \right\rangle$$

Note that $\left\langle \sum_{j=1}^N A_j^4 \right\rangle = \langle N \rangle \langle A^4 \rangle$ by Note A

We can see that $\left\langle \sum_{j \neq k}^N A_j^2 A_k^2 \right\rangle = (N^2 - N) \langle A^2 \rangle^2$ since each A_j are iid

So,

$$\left\langle \left(\sum_{j=1}^N A_j^2 \right)^2 \right\rangle = \langle N \rangle \langle A^4 \rangle + \langle N^2 \rangle \langle A^2 \rangle^2 - \langle N \rangle \langle A^2 \rangle^2$$

(c) **Note C**

Consider,

$$\left\langle \sum_{j \neq k}^N \sum_{s \neq t}^N A_j A_k A_s A_t e^{i(\theta_j - \theta_k)} e^{i(\theta_s - \theta_t)} \right\rangle$$

Most terms will equal zero except when $(\theta_j + \theta_s) - (\theta_k + \theta_t) = 0$

So, we need to consider Case 1: $s=j$ and $k=t$, Case 2: $s=t$ and $j=k$, and

Case 3: $s=k$ and $j=t$.

Case1: $s=j$ and $k=t$

Here we have $2\theta_s - 2\theta_t = 0$, but $s \neq t$ and so there is nothing to consider.

Case 2: $s=t$ and $j=k$

We made the rule that this cannot happen and thus there is nothing to consider.

Case 3: $s=k$ and $j=t$

Here we have the following:

$$\begin{aligned} & \left\langle \sum_{j \neq k}^N \sum_{s \neq t}^N A_j A_k A_s A_t e^{i(\theta_j - \theta_k)} e^{i(\theta_s - \theta_t)} \right\rangle = \\ & = \sum_{s \neq t}^N \left\langle A_s^2 A_t^2 e^{i(\theta_t - \theta_s)} e^{i(\theta_s - \theta_t)} \right\rangle \\ & = \sum_{s \neq t}^N \langle A_s^2 A_t^2 \rangle \\ & = (n^2 - n) \langle A^2 \rangle \langle A^2 \rangle \\ & = \langle N^2 \rangle \langle A^2 \rangle^2 - \langle N \rangle \langle A^2 \rangle^2 \end{aligned}$$

6. Find Intensity Squared I^2 Recall,

$$I = \sum_{j=1}^N A_j^2 + \sum_{j \neq k}^N A_j A_k e^{i(\theta_j - \theta_k)} + M^* \sum_{j=1}^N A_j e^{i\theta_j} + M \sum_{j=1}^N A_j e^{-i\theta_j} + MM^*$$

$$\begin{aligned}
I^2 &= \underbrace{\left(\sum_{j=1}^N A_j^2 \right)^2}_{P_1} + \underbrace{\left(\sum_{j \neq k}^N A_j A_k e^{i(\theta_j - \theta_k)} \right)^2}_{P_2} + \underbrace{(M^*)^2 \left(\sum_{j=1}^N A_j e^{i\theta_j} \right)^2}_{P_3} \\
&+ \underbrace{M^2 \left(\sum_{j=1}^N A_j e^{-i\theta_j} \right)^2}_{P_4} + \underbrace{M^2 (M^*)^2}_{P_5} \\
&+ 2 \left[\underbrace{\sum_{j=1}^N A_j^2 \sum_{j \neq k}^N A_j A_k e^{i(\theta_j - \theta_k)}}_{P_6} + \underbrace{M^* \sum_{j=1}^N A_j^2 \sum_{j=1}^N A_j e^{i\theta_j}}_{P_7} \right. \\
&+ \underbrace{M \sum_{j=1}^N A_j^2 \sum_{j=1}^N A_j e^{-i\theta_j}}_{P_8} + \underbrace{MM^* \sum_{j=1}^N A_j^2}_{P_9} + \underbrace{M^* \sum_{j=1}^N A_j e^{i\theta_j} \sum_{j \neq k}^N A_j A_k e^{i(\theta_j - \theta_k)}}_{P_{10}} \\
&+ \underbrace{M \sum_{j=1}^N A_j e^{-i\theta_j} \sum_{j \neq k}^N A_j A_k e^{i(\theta_j - \theta_k)}}_{P_{11}} + \underbrace{MM^* \sum_{j \neq k}^N A_j A_k e^{i(\theta_j - \theta_k)}}_{P_{12}} \\
&\left. + \underbrace{M^* M \sum_{j=1}^N A_j e^{i\theta_j} \sum_{j=1}^N A_j e^{-i\theta_j}}_{P_{13}} + \underbrace{(M^*)^2 M \sum_{j=1}^N A_j e^{i\theta_j}}_{P_{14}} + \underbrace{M^2 M^* \sum_{j=1}^N A_j e^{-i\theta_j}}_{P_{15}} \right]
\end{aligned}$$

7. **Find the Expectation of Intensity Squared $\langle I^2 \rangle$** Want to find $E[P_x]$
 $\forall x \in [1, 2, \dots, 15]$. To condition on N :

$$\langle P_1 \rangle = \left\langle \left(\sum_{j=1}^N A_j^2 \right)^2 \right\rangle = n \langle A^4 \rangle + n(n-1) \langle A^2 \rangle^2 \text{ by Note B}$$

$$\langle P_2 \rangle = \left\langle \left(\sum_{j \neq k}^N A_j A_k e^{i(\theta_j - \theta_k)} \right)^2 \right\rangle = n(n-1) \langle A^2 \rangle^2 \text{ by Note C}$$

$$\langle P_3 \rangle = \left\langle (M^*)^2 \left(\sum_{j=1}^N A_j e^{i\theta_j} \right)^2 \right\rangle = \langle (M^*)^2 \rangle \langle \sum_{j=1}^N \sum_{k=1}^N A_j A_k e^{i(\theta_j + \theta_k)} \rangle = 0 \text{ by Eq. 1}$$

$$\langle P_4 \rangle = \left\langle M^2 \left(\sum_{j=1}^N A_j e^{-i\theta_j} \right)^2 \right\rangle = \langle M^2 \rangle \langle \sum_{j=1}^N \sum_{k=1}^N A_j A_k e^{-i(\theta_j + \theta_k)} \rangle = 0 \text{ by Eq. 1}$$

$$\langle P_5 \rangle = \langle (MM^*)^2 \rangle$$

$$\langle P_6 \rangle = \left\langle \sum_{j=1}^N A_j^2 \sum_{j \neq k}^N A_j A_k e^{i(\theta_j - \theta_k)} \right\rangle = \langle \sum_{r=1}^N \sum_{j \neq k}^N A_r^2 A_j A_k e^{i(\theta_j - \theta_k)} \rangle \text{ by Eq. 1}$$

$$\langle P_7 \rangle = \left\langle M^* \sum_{j=1}^N A_j^2 \sum_{j=1}^N A_j e^{i\theta_j} \right\rangle = \langle M^* \rangle \langle \sum_{j=1}^N \sum_{k=1}^N A_j^2 A_k e^{i\theta_k} \rangle = 0 \text{ by Eq. 1}$$

$$\langle P_8 \rangle = \left\langle M \sum_{j=1}^N A_j^2 \sum_{j=1}^N A_j e^{-i\theta_j} \right\rangle = \langle M \rangle \langle \sum_{j=1}^N \sum_{k=1}^N A_j^2 A_k e^{-i\theta_k} \rangle = 0 \text{ by Eq. 1}$$

$$\langle P_9 \rangle = \left\langle MM^* \sum_{j=1}^N A_j^2 \right\rangle = \langle MM^* \rangle (n \langle A^2 \rangle) \text{ by Note A}$$

$$\langle P_{10} \rangle = \left\langle M^* \sum_{j=1}^N A_j e^{i\theta_j} \sum_{j \neq k}^N A_j A_k e^{i(\theta_j - \theta_k)} \right\rangle = \langle M^* \rangle \langle \sum_{r=1}^N \sum_{j \neq k}^N A_r A_j A_k e^{i(\theta_r + \theta_j - \theta_k)} \rangle = 0 \text{ by Eq. 1}$$

$$\begin{aligned} \langle P_{11} \rangle &= \left\langle M \sum_{j=1}^N A_j e^{-i\theta_j} \sum_{j \neq k}^N A_j A_k e^{i(\theta_j - \theta_k)} \right\rangle \\ &= \langle M \rangle \langle \sum_{r=1}^N \sum_{j \neq k}^N A_r A_j A_k e^{i(-\theta_r + \theta_j - \theta_k)} \rangle = 0 \text{ by Eq. 1} \end{aligned}$$

$$\begin{aligned} \langle P_{12} \rangle &= \left\langle MM^* \sum_{j \neq k}^N A_j A_k e^{i(\theta_j - \theta_k)} \right\rangle \\ &= \langle MM^* \rangle \langle \sum_{j \neq k}^N A_j A_k e^{i(\theta_j - \theta_k)} \rangle = 0 \text{ by Eq. 1} \end{aligned}$$

$$\begin{aligned} \langle P_{13} \rangle &= \left\langle M^* M \sum_{j=1}^N A_j e^{i\theta_j} \sum_{j=1}^N A_j e^{-i\theta_j} \right\rangle \\ &= \langle MM^* \rangle \langle \sum_{j=1}^N \sum_{k=1}^N A_j A_k e^{i(\theta_j - \theta_k)} \rangle \\ &= \langle MM^* \rangle (n \langle A^2 \rangle) \text{ by Note A} \end{aligned}$$

$$\langle P_{14} \rangle = \left\langle (M^*)^2 M \sum_{j=1}^N A_j e^{i\theta_j} \right\rangle = \langle (M^*)^2 M \rangle \langle \sum_{j=1}^N A_j e^{i\theta_j} \rangle = 0 \text{ by Eq. 1}$$

$$\langle P_{15} \rangle = \left\langle M^2 M^* \sum_{j=1}^N A_j e^{-i\theta_j} \right\rangle = \langle M^2 M^* \rangle \langle \sum_{j=1}^N A_j e^{-i\theta_j} \rangle = 0 \text{ by Eq. 1}$$

So,

$$\begin{aligned} \langle I^2 | N = n \rangle &= n \langle A^4 \rangle + 2n(n-1) \langle A^2 \rangle^2 \\ &\quad + \langle (MM^*)^2 \rangle + 4n \langle MM^* \rangle \langle A^2 \rangle \end{aligned}$$

\Rightarrow

$$\begin{aligned} \langle I^2 \rangle &= \langle N \rangle \langle A^4 \rangle + 2 \langle N \rangle^2 \langle A^2 \rangle^2 - 2 \langle N \rangle \langle A^2 \rangle^2 \\ &\quad + \langle (MM^*)^2 \rangle + 4 \langle N \rangle \langle MM^* \rangle \langle A^2 \rangle \end{aligned}$$

Recall: $N \sim \text{Poisson} \implies E[N] = \text{Var}[N] = E[N^2] - E[N]^2$

So, $\langle N \rangle = \langle N^2 \rangle - \langle N \rangle^2 \implies \langle N^2 \rangle = \langle N \rangle + \langle N \rangle^2$

\Rightarrow

$$\begin{aligned} \langle I^2 \rangle &= \langle N \rangle \langle A^4 \rangle + 2 \langle N \rangle^2 \langle A^2 \rangle^2 + \langle (MM^*)^2 \rangle \\ &\quad + 4 \langle N \rangle \langle MM^* \rangle \langle A^2 \rangle \end{aligned}$$

$$\begin{aligned} &= \langle N \rangle \langle A^4 \rangle + 2 \langle N \rangle \langle A^2 \rangle \left[\langle N \rangle \langle A^2 \rangle + 2 \langle MM^* \rangle \right] \\ &\quad + \langle (MM^*)^2 \rangle \end{aligned}$$

8. Find the Average Number of Fish $\langle N \rangle$

Note: Since $\langle I \rangle = \langle N \rangle \langle A^2 \rangle + \langle MM^* \rangle$
 $\Rightarrow \langle I \rangle - \langle MM^* \rangle = \langle N \rangle \langle A^2 \rangle$
 $\Rightarrow (\langle I \rangle - \langle MM^* \rangle)^2 = \langle N \rangle^2 \langle A^2 \rangle^2$

So,

$$\frac{\langle I^2 \rangle - \langle (MM^*)^2 \rangle}{(\langle I \rangle - \langle MM^* \rangle)^2} = \frac{\langle N \rangle \langle A^4 \rangle}{\langle N \rangle^2 \langle A^2 \rangle^2} + \frac{2\langle N \rangle^2 \langle A^2 \rangle^2}{\langle N \rangle^2 \langle A^2 \rangle^2} + \frac{4\langle N \rangle \langle A^2 \rangle \langle MM^* \rangle}{\langle N \rangle^2 \langle A^2 \rangle^2}$$

$$= \frac{\langle A^4 \rangle}{\langle N \rangle \langle A^2 \rangle^2} + 2 + 4 \frac{\langle MM^* \rangle}{\langle N \rangle \langle A^2 \rangle}$$

\Rightarrow

$$\frac{\langle I^2 \rangle - \langle (MM^*)^2 \rangle}{(\langle I \rangle - \langle MM^* \rangle)^2} - 2 = \frac{1}{\langle N \rangle} \left[\frac{\langle A^4 \rangle}{\langle A^2 \rangle^2} + 4 \frac{\langle MM^* \rangle}{\langle A^2 \rangle} \right]$$

\Rightarrow

$$\langle N \rangle = \left[\frac{\langle A^4 \rangle}{\langle A^2 \rangle^2} + 4 \frac{\langle MM^* \rangle}{\langle A^2 \rangle} \right] \left[\frac{\langle I^2 \rangle - \langle (MM^*)^2 \rangle}{(\langle I \rangle - \langle MM^* \rangle)^2} - 2 \right]^{-1}$$

APPENDIX B

DERIVATION OF PROBABILITY DENSITY FUNCTION OF THE FISH SCATTERING STATISTIC AND BEAM PATTERN MODULATION

Appendix B-1: Derivation of Fish Scattering Effects

For this research the fish scattering statistic, a , is assumed to follow a Rayleigh distribution with parameter σ representing the mode. The Rayleigh pdf is

$$\rho(x; \sigma) = \frac{x}{\sigma^2} e^{-x^2/2\sigma^2},$$

for $x \geq 0$. Thus the raw moments are given by:

$$\langle a^k \rangle = \sigma^k 2^{\frac{k}{2}} \Gamma(1 + \frac{k}{2})$$

such that:

$$\begin{aligned}\langle a \rangle &= \sqrt{\frac{\pi}{2}} \sigma \\ \langle a^2 \rangle &= 2\sigma^2 \\ \langle a^3 \rangle &= 3\sqrt{\frac{\pi}{2}} \sigma^3 \\ \langle a^4 \rangle &= 8\sigma^4.\end{aligned}$$

Thus, the fourth normalized moment of the fish scattering statistic, a , is equal to,

$$\begin{aligned}\langle a^4 \rangle / \langle a^2 \rangle^2 &= 8\sigma^4 / (2\sigma^2)^2 \\ &= 8\sigma^4 / 4\sigma^4 \\ &= 2.\end{aligned}$$

Appendix B-2: Derivation of Beam Pattern Effects (As seen in Peterson *et. al.* [1976])

(The setup for the work done in this research is the third scenario)

1. Setup for a transducer with axial symmetry about the z -axis (As seen in Appendix Figure 1.1):

Here $r > 0$ and $0 \leq \phi \leq \pi/2$. The goal is to find the probability density of the location of the fish producing single echoes. Thus, given some range, r , the random variable is Φ .

This method assumes that the fish are uniformly distributed in space

\implies A ratio of volumes can be considered to find $\rho_{\Phi}(\phi)$. The numerator is the volume of the cylindrical shape with some radius, r' , and height, dr . The denominator is the volume of the hemi-spherical shell.

$$\implies \rho_{\Phi}(\phi) = \frac{V_{cylinder}}{V_{hemi-spherical\ shell}} = \frac{\Delta V}{V_{hemi-spherical\ shell}}$$

To find $V_{cylinder}$, the area of the small sector is subtracted from the area of the large sector (Appendix Figure 1.2) and then multiplied by $2\pi r'$, where r' is the radius of the cylinder. This can be done due to the axial symmetry of the setup.

$$\begin{aligned} (\text{Large Sector}) - (\text{Small Sector}) &= [\pi(r + \frac{dr}{2})^2(\frac{d\phi}{2\pi})] - [\pi(r - \frac{dr}{2})^2(\frac{d\phi}{2\pi})] \\ &= \frac{\pi d\phi}{2\pi} [(r^2 + 2r\frac{dr}{2} + \frac{(dr)^2}{4}) - (r^2 - 2r\frac{dr}{2} + \frac{(dr)^2}{4})] \\ &= \frac{\pi d\phi}{2\pi} (2r dr) \end{aligned}$$

$$\text{Thus } \Delta V = V_{cylinder} = 2\pi r'(\frac{\pi d\phi}{2\pi} 2r dr) = 2\pi r' r d\phi dr.$$

$$\text{Notice that } r' = r \sin \phi \implies \Delta V = 2\pi r^2 \sin \phi d\phi dr.$$

Thus,

$$\begin{aligned} V_{hemi-spherical\ shell} &= \int_0^{\pi/2} \Delta V \\ &= \int_0^{\pi/2} 2\pi r^2 \sin \phi dr d\phi \\ &= 2\pi r^2 dr [-\cos \phi]_0^{\pi/2} \\ &= 2\pi r^2 dr \end{aligned}$$

Therefore,

$$\rho_{\Phi}(\phi) = \frac{\Delta V}{V_{\text{hemi-spherical shell}}} = \frac{2\pi r^2 \sin \phi d\phi dr}{2\pi r^2 dr} = \sin \phi d\phi$$

is the pdf of the fish scatterer position in space.

In order to estimate the effects of the beam pattern on the estimate of the average number of fish, a “beam pattern probability density function” needs to be found. Since the beam pattern is dependent on a random variable, Φ , the beam pattern itself is considered a random variable.

The typical transformation would be: $\rho_B(b) = \frac{\rho_{\Phi}(\phi(b))}{\left|\frac{db}{d\phi}\right|_{\phi(b)}}$ for $0 \leq b \leq 1$ where B represents the random variable of the beam pattern.

In this situation the pdf can be represented by

$$\rho_B(b) = \frac{1}{\Delta b} \int_{\Delta\phi'} \rho_{\Phi}(\phi'),$$

where $\Delta\phi'$ represents the limits for all the angles for which b is bounded by $\tilde{b} \pm \frac{\Delta b}{2}$.

2. Setup for a transducer with two angle dependencies (As seen in Figure 2 of the main document):

Here $0 > r$, $0 \leq v \leq 2\pi$, $0 < \phi < \pi/2$. Again, want to find the probability density of the location of the fish producing echoes. Given a range, r , the two random variables are Υ and Φ .

As before, it is assumed that the fish are uniformly distributed in space.

\implies A ratio of volumes can be considered to find $\rho_{\Phi,\Upsilon}(\phi, v)$. Although the denominator is the same volume as considered in the previous setup, the volume in the numerator is found from the cube seen in Figure 2 (main document) due to the addition of a second angle dependency.

$$\implies \rho_{\Phi,\Upsilon}(\phi, v) = \frac{V_{\text{cube}}}{V_{\text{hemi-spherical shell}}} = \frac{\Delta V}{V_{\text{hemi-spherical shell}}}$$

$$\begin{aligned} V_{cube} &= r \sin \phi dv r d\phi dr \\ &= r^2 \sin \phi d\phi dv dr \end{aligned}$$

$$\begin{aligned} V_{hemi-spherical\ shell} &= \int_0^{2\pi} \int_0^{\pi/2} V_{cube} \\ &= \int_0^{2\pi} \int_0^{\pi/2} (r^2 \sin \phi dr) d\phi dv \\ &= r^2 dr \int_0^{2\pi} dv \int_0^{\pi/2} \sin \phi d\phi \\ &= r^2 dr 2\pi [-\cos \phi]_0^{\pi/2} \\ &= 2\pi r^2 dr \end{aligned}$$

Therefore,

$$\rho_{\Phi, \Gamma}(\phi, \nu) = \frac{\Delta V}{V_{hemi-spherical\ shell}} = \frac{r^2 \sin \phi d\phi dv dr}{2\pi r^2 dr} = \frac{\sin \phi}{2\pi} d\phi dv$$

Note: This can be verified by applying the axial symmetry assumption and comparing the results to number 1.

If there is axial symmetry in the setup then $\rho_{\Phi, \Gamma}$ can be integrated with respect to ν from 0 to 2π .

Thus,

$$\int_0^{2\pi} \rho_{\Phi, \Gamma}(\phi, \nu) = \int_0^{2\pi} \frac{\sin \phi}{2\pi} d\phi dv = 2\pi \frac{\sin \phi}{2\pi} d\phi = \sin \phi d\phi = \rho_{\Phi}(\phi) \quad \checkmark$$

The following transformation can then be applied to find the “beam pattern pdf:”

$$\begin{aligned} \rho_B(b) &= \frac{1}{\Delta b} \int_{\Delta \nu'} \int_{\Delta \phi'} \rho_{\Phi, \Gamma}(\phi, \nu) \\ &= \frac{1}{\Delta b} \int_{\Delta \nu'} \int_{\Delta \phi'} \frac{\sin \phi'}{2\pi} d\nu' d\phi' \end{aligned}$$

where $\Delta \phi'$ and $\Delta \nu'$ represent the limits for all the angles for which b is bounded by $\tilde{b} \pm \frac{\Delta b}{2}$.

3. Setup for a transducer with two angle dependencies with an added stipulation (As seen in Appendix Figure 2):

It is assumed that the fish have a uniform distribution in some restricted area in space (rather than being uniform on $0 < v < 2\pi$ and $0 < \phi < \pi/2$, the fish are now uniform on $0 < v < 2\pi$ and $0 < \phi < \alpha$). Only angles within the “cone” defined by α are considered to be part of the uniform spatial distribution.

A ratio of volumes can be considered where the numerator is the volume of the cube and the denominator is the volume of the cone.

Recall that the volume of the cube is $V_{cube} = r^2 \sin \phi d\phi dv dr$, thus,

$$\rho_{\Phi, \Upsilon}(\phi, v) = \frac{V_{cube}}{V_{cone}} \quad \text{where}$$

$$\begin{aligned} V_{cone} &= \int_0^v \int_0^{2\pi} V_{cube} \\ &= \int_0^v \int_0^{2\pi} (r^2 \sin \phi dr) dv d\phi \\ &= 2\pi r^2 dr [-\cos \phi]_0^\alpha \\ &= 2\pi r^2 dr [1 - \cos \alpha] \end{aligned}$$

Therefore,

$$\rho_{\Phi, \Upsilon}(\phi, v) = \frac{V_{cube}}{V_{cone}} = \frac{r^2 \sin \phi d\phi dv dr}{2\pi r^2 dr [1 - \cos \alpha]} = \frac{\sin \phi}{2\pi(1 - \cos \alpha)} d\phi dv$$

$$\implies \rho_B(b) = \frac{1}{\Delta b} \int_{\Delta\phi'} \int_{\Delta v'} \frac{\sin \phi'}{2\pi(1 - \cos \alpha)} dv' d\phi'$$

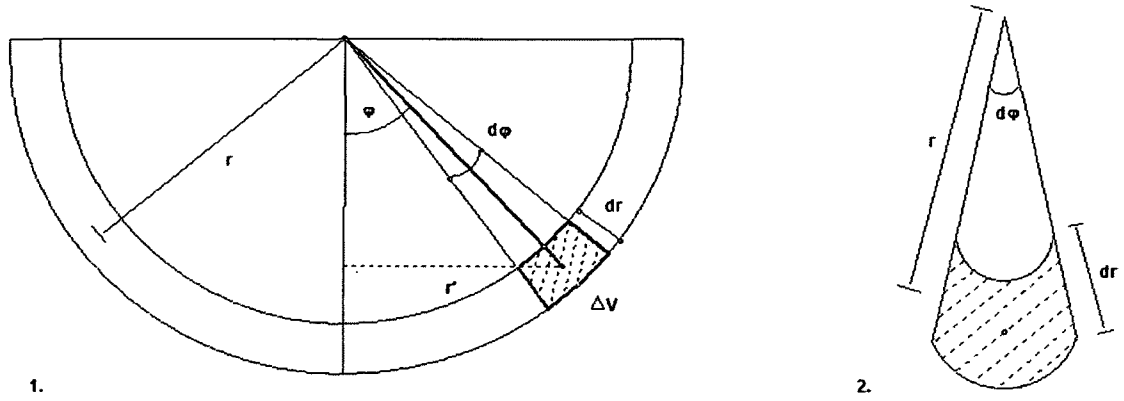


Figure B-1. 1. Geometry of backscattered pressure signal for setup number one. 2. Vertical slice of cylindrical shape used to find area.

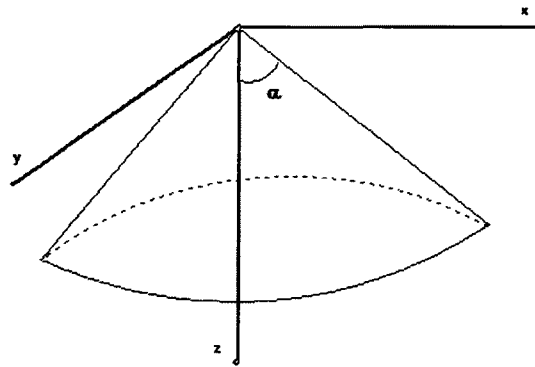


Figure B-2. Geometry of backscattered pressure signal for setup number three.

APPENDIX C

VARIANCE OF $\langle N \rangle$

A general expression for the variance of the scintillating index of intensity, $\frac{\langle I^2 \rangle}{\langle I \rangle^2}$, with negligible noise was derived in Denbigh et. al. [1991] to be:

$$\begin{aligned} Var(SI) &= Var\left(\frac{\langle I^2 \rangle}{\langle I \rangle^2}\right) \\ &= \frac{1}{m} \left[\frac{\langle I^4 \rangle}{\langle I \rangle^4} - 4 \left(\frac{\langle I^3 \rangle}{\langle I \rangle^3} \frac{\langle I^2 \rangle}{\langle I \rangle^2} \right) + 4 \left(\left(\frac{\langle I^2 \rangle}{\langle I \rangle^2} \right)^3 - \left(\frac{\langle I^2 \rangle}{\langle I \rangle^2} \right)^2 \right) \right] \end{aligned}$$

where m is the number of independent samples. This was used to determine $Var(\langle N \rangle)$:

$$Var(\langle N \rangle) = \langle N \rangle^2 Var\left(\frac{\langle I^2 \rangle}{\langle I \rangle^2}\right)^{1/2} \left[\frac{\langle a^4 \rangle}{\langle a^2 \rangle^2} \frac{\langle b^4 \rangle}{\langle b^2 \rangle^2} \right]^{-1}$$

where $\frac{\langle a^4 \rangle}{\langle a^2 \rangle^2} \frac{\langle b^4 \rangle}{\langle b^2 \rangle^2}$ is assumed to be constant. It is important to note that, for this model, the fourth normalized moment of the pulse envelope is equal to one.

To account for possible noise contributions, a new estimate for $Var(\langle N \rangle)$ is derived below for the variant model, (Eq. 9).

As done in Denbigh et. al. [1991], let

$$X = \langle I^n \rangle - \langle (MM^*)^n \rangle, \quad Y = \langle I \rangle - \langle MM^* \rangle, \quad \text{and} \quad n = 2$$

such that

$$Z = [\langle I^n \rangle - \langle (MM^*)^n \rangle][\langle I \rangle - \langle MM^* \rangle]^{-n} = XY^{-n}$$

Then,

$$Var(Z) = \left(\frac{\partial Z}{\partial X}\right)^2 Var(X) + \left(\frac{\partial Z}{\partial Y}\right)^2 Var(Y) + 2\left(\frac{\partial Z}{\partial X}\right)\left(\frac{\partial Z}{\partial Y}\right) Cov(X, Y)$$

where $Var(A)$ is the variance in the random variable A , and $Cov(A, B)$ is the covariance of A and B (Papoulis 1965).

$$\begin{aligned} \implies Var(Z) &= (Y^{-n})^2 Var(X) + (-nXY^{-(n+1)})^2 Var(Y) \\ &\quad + (-2nXY^{-(2n+1)}) Cov(X, Y) \\ &= \frac{Var(X)}{(\langle I \rangle - \langle MM^* \rangle)^{2n}} + Var(Y) \left(\frac{n(\langle I^n \rangle - \langle (MM^*)^n \rangle)}{(\langle I \rangle - \langle MM^* \rangle)^{(n+1)}} \right)^2 \\ &\quad - \frac{2n(\langle I^n \rangle - \langle (MM^*)^n \rangle)}{(\langle I \rangle - \langle MM^* \rangle)^{(2n+1)}} Cov(X, Y) \end{aligned}$$

It is important to note that

$$\begin{aligned} Var(X) &= Var(\langle I^n \rangle - \langle (MM^*)^n \rangle) \\ &= Var(\langle I^n \rangle) + Var(\langle (MM^*)^n \rangle) - 2Cov(\langle I^n \rangle, \langle (MM^*)^n \rangle) \\ &= \frac{1}{m}(\langle I^{2n} \rangle - \langle I^n \rangle^2) + \frac{1}{m}(\langle (MM^*)^{2n} \rangle - \langle (MM^*)^n \rangle^2) \\ &\quad - 2Cov(\langle I^n \rangle, \langle (MM^*)^n \rangle) \end{aligned}$$

and

$$\begin{aligned} Var(Y) &= Var(\langle I \rangle - \langle MM^* \rangle) \\ &= Var(\langle I \rangle) + Var(\langle MM^* \rangle) - 2Cov(\langle I \rangle, \langle MM^* \rangle) \\ &= \frac{1}{m}(\langle I^2 \rangle - \langle I \rangle^2) + \frac{1}{m}(\langle (MM^*)^2 \rangle - \langle MM^* \rangle^2) \\ &\quad - 2Cov(\langle I \rangle, \langle MM^* \rangle) \end{aligned}$$

since $Var(A) = E(A^2) - (E(A))^2$ for a random variable A . For two random variables A and B the covariance term is equal to the following:

$$Cov(A, B) = E(AB) - E(A)E(B).$$

Recalling that if A and B are uncorrelated, then $Cov(A, B) = 0$.

For the purposes of this research, the moments of intensity are assumed to be uncorrelated to the moments of noise. Thus,

$$\begin{aligned} Var(X) &= \frac{1}{m}(\langle I^{2n} \rangle - \langle I^n \rangle^2) + \frac{1}{m}(\langle (MM^*)^{2n} \rangle - \langle (MM^*)^n \rangle^2) \\ Var(Y) &= \frac{1}{m}(\langle I^2 \rangle - \langle I \rangle^2) + \frac{1}{m}(\langle (MM^*)^2 \rangle - \langle MM^* \rangle^2) \end{aligned}$$

and

$$\begin{aligned}
Cov(X, Y) &= Cov(\langle I^n \rangle - \langle (MM^*)^n \rangle, \langle I \rangle - \langle MM^* \rangle) \\
&= E[(\langle I^n \rangle - \langle (MM^*)^n \rangle)(\langle I \rangle - \langle MM^* \rangle)] \\
&\quad - E[\langle I^n \rangle - \langle (MM^*)^n \rangle]E[\langle I \rangle - \langle MM^* \rangle] \\
&= E[(\langle I^n \rangle - \langle (MM^*)^n \rangle)(\langle I \rangle - \langle MM^* \rangle)] \\
&\quad - (\langle I^n \rangle - \langle (MM^*)^n \rangle)(\langle I \rangle - \langle MM^* \rangle) \\
&= E[\langle I^n \rangle \langle I \rangle - \langle I^n \rangle \langle MM^* \rangle - \langle I \rangle \langle (MM^*)^n \rangle \\
&\quad - \langle MM^* \rangle \langle (MM^*)^n \rangle] \\
&\quad - (\langle I^n \rangle - \langle (MM^*)^n \rangle)(\langle I \rangle - \langle MM^* \rangle)
\end{aligned}$$

can be used to find $Var(Z)$ and therefore the estimate of $Var(\langle N \rangle)$ using the formula derived in Denbigh et. al. [1991].